Estimation of Empirical Rainfall Thresholds for Landslide Triggering Using Partial Duration Series and Their Relation with Climatic Cycles. An Application in Southern Ecuador

John Soto(1,3), José Antonio Palenzuela(2), Jorge P. Galve(3), Juan Antonio Luque (4), José Miguel Azañón(2), José Tamay(1), Clemente Irigaray(3)

(1) Departamento de Geología y Minas e Ingeniería Civil, Universidad Técnica Particular de Loja, Loja, Ecuador, Ap. 1101608

(2) Department of Civil Engineering, ETSICCP, University of Granada, Campus Fuentenueva s/n, Granada 18071, Spain.

(3) Departamento de Geodinámica, Facultad de Ciencias, Universidad de Granada, 18071, Granada, Spain

(4) Instituto Geológico y Minero de España. Urb. Alcázar del Genil, 4 bajo. Edificio Zulema. 18006 Granada.

ABSTRACT

Rainfall-induced landslides constitute a major cause of damage and fatalities throughout the intramontane basins of the Andes. The geological and climatic setting plays a key role in the generation of a high number of landslides in this area. For this reason, a greater understanding of the relationship between landslide frequency and climate conditions is necessary to mitigate human and economic losses. Accordingly, this paper presents an analysis of rainfall variables associated with a series of dated landslides (153 in total) in the southern Ecuador basin of Loja. This analysis was performed by applying an affordable empirical method that enables the calculation of Critical Rainfall Threshold (CRT) curves. This calculation is based on an in-depth examination of rainfall parameters, such as cumulative precipitation and mean intensity, linked to a wide range of rainfall duration (from 1 to 90 days). The inspection of these parameters was addressed considering their frequency, which was calculated by using Partial Duration Series (PDS), taking into account the entire rainfall record. This work has revealed that only 24% of landslides were triggered by rainfall conditions with maximum return periods greater than 1 year, whereas the rest did not exceed that return period. After finding the best correlation between the maximum return periods and the maximum mean intensity, a minimum power law function was adjusted to the CRT curve that correlates duration and cumulative rainfall. The values for this CRT function resulted in 5,14 and 0,83 for its scaling constant (α) and shape parameter (β), respectively. In addition, a spectral analysis was conducted to detect climatic cycles on the entire rainfall record. In general, a clear correlation could not be established between climatic frequencies and significant rainfall events

inducing landslides, although similarly return periods were found for a critical rainfall event of March 2015 (10,4 y) and the SUNSPOT cycles (10,5-12y) . The results derived from this research are significantly valuable for the prevention of future mass-movements, although additional data will be crucial to update and calibrate CRT curves to study the influence of climate on landslide event frequency and magnitude in Loja.

Keywords:

Return period; Rainfall threshold; Landslides; Spectral analysis; Climatic cycles

1. Introduction

Landslides occur frequently as a consequence of intensive rainfall. These geomorphic processes generate risk situations and sometimes lead to disasters with magnitudes similar to those of other natural hazardous phenomena. The destructive potential of mass movements increases with the urban development of landslide-prone areas (Aleotti and Chowdhury 1999; Guzzetti et al. 1999). Thus, the damage due to landslides in human and monetary terms is rising because of the urban growth observed in cities located in mountain settings. This trend is evident in the data compiled in the literature specialized in landslide events (e.g., Unesco 1973-79; Brabb 1991; Guzzetti et al. 1999; Schuster and Highland 2001; Cardinali et al. 2002; Haque and Burton 2005; Petley et al. 2005; Nadim et al. 2006; Lacasse and Nadim 2009; Petley 2012; Shanmugam 2015; Gariano and Guzzetti, 2016). For example, Brabb (1991) estimated an increase of 600 landslides per year until reaching several thousands of landslides per year by the early 1990's. This is coincident with the figure quantified by Petley (2012) of 2620 fatal landslides from 2004 to 2010 (both inclusive), which caused 32.332 fatalities Many of these landslides occurs in high mountains that are tectonically active. From these events, those causing the majority of human losses occurred in Asia, especially in China and along the Himalayan Arc (Petley et al. 2007; Petley 2012, Runqiu 2009; Mauri and Wanfg 2015; Sassa et al. 2015; Song et al. 2015; Hung et al. 2016; Xu et al. 2017), as consequence of extreme rainfall, earthquakes or snow melt events. Hotspots with moderate to very high landslide hazard have been also identified in the United States Burns (2014), where many of the urban landslides produce until 25-50 deaths per year and about $3,5 billion in damage.
Landslides are one of the most serious threats that the Andean community faces (Hermanns, 2012). It can be seen from the data in Table 1 that important rainfall-triggered landslides in the Andes have led to losses of millions of dollars and thousands of fatalities. In particular, landslides are the natural hazard with the widest impact in Ecuador, where this research was conducted. According to Eras (2014), in Ecuador between 1970 and 2013, 3113 slope movement events occurred (Fig. 1a). These mass movements occurred during the most humid months: January, February, March and April (Fig. 1b). Other reports state that during the period of 1970-2010, 19% of the 5523 events associated with different natural hazards in Ecuador were mass movements, and this type of

phenomenon caused the greatest number of victims and economic losses (SNGR/ECHO/UNISDR, 2012). Moreover, landslides commonly disturb the social and economic activity of Ecuadorian populations because they are the cause of frequent road blocks, power outages, and other problems. Guayas and Loja are two provinces that especially suffer the impact of these processes (SNGR/ECHO/UNISDR, 2012).

Table 1. Landslides with major damage caused in the Andean region, triggered by rainfall

Figure 1. a) Annual distribution of landslides generated in Ecuador (1970 – 2013) showing El Niño–Southern Oscillation (ENSO) events; b) Relationship between the number of landslides and the mean monthly precipitation (1970 – 2011) (Eras, 2014).

Currently, both developing and developed countries have problems in covering the costs of the damage as well as slope stabilization measures. This global situation has led to a strategy in which prevention supported by risk models, early warning systems and land use planning constitutes the most suitable method for minimizing human and economic losses due to landslides (Aleotti and Chowdhury 1999; Chacón et al. 2006). This demonstrates the importance of estimating the probability of landslide occurrence in a given area for a certain time frame of planning. To this end, data of landslide location, frequency and triggering factors (i.e., rainfall) must be compiled. Thus, many programmes or projects devoted to the reduction of losses due to landslides are dedicated to assembling landslide inventories and integrating them with time-series analysis of precipitation data (Casale et al. 1994; Dikau et al. 1996; Panizza 1996; Van Den Eeckhaut and Hervás 2012). The aim of such integration is to estimate the so-called critical rainfall threshold (CRT), which refers to the rainfall amount and/or intensity that triggers landslides in a specific area (e.g., Lumb 1975; Crozier and Eyles 1980; Crozier 1986; Kim et al. 1991; Terlien 1996; Terlien 1998; Glade et al. 2000; Wieczorek and Glade 2005; Guzzetti et al. 2007; Guzzetti et al. 2008; Palenzuela et al. 2016). There are two main procedures for estimating CRTs: (1) applying physical models driven by hydrogeological and geotechnical parameters (Borga et al. 2002; Aleotti and Polloni 2003; Frattini et al. 2004; Li et al. 2011; De vita et al. 2013; Papa et al. 2013; Ma et al. 2014); (2) empirical analysis of the relationship between historical records of precipitation and landslides (Lumb 1975; Crozier and Eyles 1980; Crozier 1986; Kim et al. 1991; Terlien 1996; Terlien 1998; Glade et al. 2000; Wieczorek and Glade 2005; Guzzetti et al. 2007; Guzzetti et al. 2008; Palenzuela et al. 2016). The second option requires an exhaustive compilation of historical information and a detailed rainfall record, but it may be more affordable than the physical modelling, as in-situ mechanical and laboratory testing is not necessary. By using experimental methods, different thresholds have been determined at the global, regional and local scale (Caine 1980, Rossi et al. 2006; Guzzetti et al. 2008). This type of research focuses in determining indicative parameter (e.g. intensity – duration or I-D) of the rainfall amount needed to trigger a landslide. In regard to regions of the above mentioned countries, hardly affected by landslides, examples of scientific works can be referred here. For instance, Saito et al. (2010) conducted a regional analysis on the I-D rainfall conditions for landslide triggering in Japan, beginning from both radar and raingauges measures. Zhuang et al. (2017) applied the quantitative model of TRIGRS (Transient Rainfall Infiltration and Grid-based Regional Slope-Stability) by using parameters related to the 12 July 2013 extreme rainfall event at Yan'an (Northwest China). They attemped to predict the spatial and temporal occurrence of landslides, validating their findings with the knowledge about the landslides caused by the same rainfall event. Kumar et al. (2017) studied the rainfall conditions by analysing the cumulative rainfall. They selected homogeneous time series from July to September for the Jammu and Kashmir Himalaya, enabling the correlation of extreme events with landslides occurrences. This study revealed abnormal rainfall patterns when considering 1 to 7 days of continuous rainfall at the beginning or the withdrawal of the Indian Summer Monsoon. For the case of the United States of America, Baum and Godt (2010) used different research findings to study the variability of the rainfall thresholds of different regions. They expressed these thresholds as a function of the intensity and duration, as well as the antecedent precipitation followed by landslide occurrence.

In the Andean region, landslides have been studied through geotechnical (e.g., Wilcke et al. 2003; Bussman et al. 2008; Soto et al., 2017) and environmental (e.g., Lozano et al. 2005, Muenchow et al. 2012) points of view. In addition, recent susceptibility analysis based on advanced statistical analysis (Brenning et al. 2015) has been applied. However, published estimations of CRTs in the Andes are scarce (e.g., Terlien 1996; Terlien 1997; Terlien 1998; González and Mayorga 2004; Aristizábal et al. 2016), although this information is essential for conducting sound landslide hazard and risk assessments.

This research focuses in the estimation of empirical critical rainfall threshold triggering landslides in the Loja city, the capital of the Loja province, Ecuador. In addition, it is also aimed at detecting and comparing climatic cycles with the recurrence of critical rainfall thresholds producing a significant number of landslides in the study area. In this city, landslides are frequently triggered by hydro-meteorological phenomena and conditioned by the strong weathering of the bedrock and high clay content of the soils (Soto et al., 2017). According to this statement, the hydrological conditions were analysed by using partial duration series to generate numerous time series on the cumulative rainfall frequency. This processing of rainfall data was followed by the definition of critical rainfall thresholds associated with 153 landslides that occurred during the last decade in the study area. Finally, the return periods of significant rainfall events were compared with the recurrence of climatic cycles. Therefore, this research will entail a step forward in landslide hazard assessment, attempting to generate fundamental information on hydrometeorological events associated with the occurrence of major landslides in this region.

2. Study area

The geographical setting makes the city of Loja an excellent place to carry out time-series analyses for correlating rainfall with landslide occurrence. Loja is located in a wide valley at 2100 m a.s.l. in southern Ecuador, between the meridians 79º10’ and 79º15’ and between the parallels 3º55’ and 4º5’. Most of these landslides are usually rainfall-induced, and they are influenced by low strength properties of the rocks that outcrop in the bottom and lower slopes of the valley (Ibadango et al. 2005; Soto et al. 2017). Loja basin shows humid subtropical climate because of its latitude and elevation. The average annual rainfall is 917 mm, and the average monthly temperature is 16.2 °C. The period with a lower average temperature extends from June to September, with July being the coldest month (14.9 °C) (ML PNUMA 2007). The most intensive rainfall is concentrated from December to April, the so-called humid season, but precipitation continues throughout the year. The humid season is characterized by strong storms and high precipitation periods that trigger floods, torrent-related phenomena and landslides.

2.1 Geology

Loja is located in the Loja Basin, one of the intramontane basins of Southern Ecuador (Fig. 2a). This basin was developed over a metamorphic basement composed of fine- to medium-grain quartzites, dark phyllites, shales, and schists of Paleozoic age (Fig. 2b). The fill of the basin corresponds to Miocene-Pliocene sediments affected by a moderate deformation. The Neogene sedimentary sequence was established by Kennerley (1980) and studied in detail by Hungerbühler et al. (2002). The sequence, from bottom to top, comprises (1) coarse grain sandstones with thin layers of conglomerates and mudstones of the Trigal Formation; (2) limestones, thin layers of carbonate mudstones, layers of chert (silica) and yellow sandstones of the La Banda Formation; (3) layers of sandstones intercalated with conglomerates of the Belen Formation; (4) sandstones, carbonaceous and siliceous mudstones, diatomites, lignites, and conglomerate intercalations of San Cayetano Formation; (5) conglomerates of Quillollaco Formation; and (6) heavily weathered lithic tuffs of the Salapa Formation of pyroclastic origin (volcanic). The San Cayetano, Belén and Trigal formations show high clay mineral content of the smectite group (Soto et al. 2017). These minerals confer very high plasticity to these materials and contribute to the ground instability observed in Loja. The expansive behaviour of these clays, enhanced by the tropical climate, allows for low gradient slopes (10–15°) that can also slide. This characteristic causes large parts of the Loja Valley to be susceptible to landslides (Soto et al. 2017).

Figure 2. Geographical and geological setting of the study area: a) Ecuador regions and landslide inventory (INIGEMM, 2013); b) Geological formations of the study area.

2.2 Geomorphology

The landscape of the Loja Valley is controlled by the tilted and folded layers of the Loja Basin infill sediments. Landforms in the valley are mainly north-south oriented. The valley is anomalously wide (7 km-average and 14 km-maximum). At West, it is bounded by the uplifted metamorphic rocks of the Villonaco Range. This range consists of a lower mountain chain with elevations of approximately 2700 m a.s.l.. The bottom of the valley is formed predominately by low hills or ‘cuesta’ landforms and a colluvium covering the NW area. At East, the limit of the valley show a sierra with peaks that reach more than 3200 m a.s.l. which forms part of the Oriental Range of Andes (Fig. 2b).

This rugged terrain is partially covered by Ecuador's ninth largest city, Loja (170,280 inhabitants, INEC, 2010). The urban sprawl of this city in the last decades occurred outside of the most stable terrain, encroaching on the slopes of the hills in the bottom of the valley. In many cases, the promoters of urban development underestimated the instability problems of these slopes and several landslides have affected the new neighbourhoods, causing extensive damage and even fatalities (cf. Soto et al., 2017).

3. Deployed data: Landslide catalogue and precipitation series

To apply the methodology proposed in this paper, two datasets were needed: a catalogue of rainfall-triggered landslides with temporal and spatial information and a daily precipitation series. Thus, the latter dataset represents the triggering factor of the catalogued landslides, which can be used in a back analysis with the aim of found critical rainfall events triggering landslides.

The landslide catalogue comprises dates and locations of landslides in Loja between 2006 and 2015 (Fig. 3). However, the lack of information and data limits the accuracy and completeness of this historical database (Ibsen y Brunsden 1996, Palenzuela et al. 2016). For instance, although newspapers are published from longer periods, landslide records start being more continuous and detailed from the last decades (Corominas and Moya 2008). There is also some available information on landslides events in official institutions, but bureaucratic processes delayed the access to unpublished reports. When referring to landslides inventories the lack of data is commonly linked to the low resolution of aerial photographs or satellite images but also to the subjectivity and working experience of the cartographer. These are possible factors explaining the increase in the number of landslides dated since 2011 in our database (Fig. 3). This affects the global trend of the rainfall thresholds triggering landslides. Specifically, Gariano et al. (2015) found that even a small (1%) underestimation in the number of registered landslides can result in a significant error in the effectiveness of a threshold-based prediction model. As a result, landslides occurring during lower rainfall thresholds can be omitted, generating false negative errors (a missing alert when a true risk of landslide is coming up). On the contrary, the geographical distance between each rainfall-measurement station and landslides can result in an underestimation of thresholds for landslide triggering (Nikolopoulos et al. (2014). This could lead to false positives (alerting after rainfall amounts bellow a critical limit are reached).

In this investigation a landslide catalogue was compiled through the revision of files from the Ecuadorian Secretary for Risk Management (SNGR) and news in the written and digital press, mainly in the "La Hora" and the "El Comercio" newspapers. The search in the newspaper archives provided information about the damage between 2006 and 2013 from 46 landslides. The SNGR files reported 240 landslides in the Loja province for the period of 2010 – 2015, among which 167 occurred in the study area, and 153 included date and location data. The reports of the SNGR-Zone 7, documented 240 slope movements. These reports indicated that 70% of the landslides documented in the Loja province (11,063 km^2) occurred in Loja Valley (108 km^2). A total of 1911 people were directly or indirectly affected by these landslides, and 243 homes were damaged, for a total loss of 4 million USD. In addition, 7 people lost their lives because of landslides in the city of Loja between 2010 and 2015 (Table 2). Overall, 90.4% of the reported landslides were triggered by rainfall events (Fig. 4). Most of these landslides (85%) are of complex, earth-slide or earth-flow type (Fig. 5), according to the classification of Cruden and Varnes (1996). In general, they consist of very slow creep movements that evolve into flows after high precipitation events. The analysis here was focused on these types of landslides because they are the most common and damaging in the study area.

Table 2. Reported damage due to landslides in the Loja basin between 2010 and 2015 (SNGR – Zona 7)

Figure 3. Annual distribution of landslides in Loja that occurred between 2006 and 2015

Figure 4. Main triggers of landslides in southern Ecuador and monthly distribution of the catalogued landslides (2010 – 2015). Black bars represent the number of landslides by month, while yellow bars represent the number of landslides by trigger type

Figure 5. Landslide inventory in the study area (green polygons) and photographs of predominant types

There are currently 7 meteorological stations in the Loja basin. One of these stations belongs to the INAMHI (Instituto Nacional de Meteorología e Hidrología), it is called "La Argelia" and was placed in the 60s. The other 6 stations belong to the UTPL (Universidad Técnica Particular de Loja) and were recently placed in 2011. Given its longer rainfall record, the "La Argelia" meteorological station was used in this research. This station is located in the South of the Loja Valley at 2160 m a.s.l., at latitude 4º 01´50´´ S and length of 79º 11´58´´ W. The precipitation series consisted of 24h-rainfall amounts collected by a rain gauge during a period of 52 years from 1 January 1964 to 30 September 2015.

4. Methods

The methodology applied in this research deals with two major matters. First, an empirical method is applied to search the critical rainfall variables (duration, accumulated rainfall, and mean intensity) and their return period associated with every rainfall event that causing catalogued landslides. Therefore, this collection of rainfall data will enable the building of Critical Rainfall Threshold (CRT) curves. Furthermore, knowing the impact of climate phenomena on floods and landslides another interesting part of this methodology was developed. It consisted of detecting climate cycles for the study area and then comparing their recurrence with the return periods of important rainfall events causing landslides. This part of the methodology was based on a spectral analysis that was applied to the whole rainfall record. The research methodology was developed by the following stages, matching the order numbers in the flow diagram in Figure 6:

1) Assuming that a landslide event can be associated with a rainfall event of a high return period, a high number of C_i- D_i combinations will enable the selection of the highest return period for every landslide event (Segoni et al. 2013). Thus, in this research a high number of time-series on the cumulative precipitation (C_i) was calculated for different durations (D_i) of the rainfall event by using a VBA macro created in an Excel file. As described in Section 2, the humid subtropical climate of the Loja basin and its continued rain throughout the whole year suggests that soil and rocks will keep a high saturation level in time, providing the water as a conditioning factor during every season. Accordingly, shorter periods (days, weeks or several months) of rainfall events were considered here to increase the pore water pressure and trigger landslides. Based on this assumption, D_i-values were set from 1 to 90 days. Thus, a new set of 90 time series was generated for every rainfall row of the daily rainfall database.
2) Before obtaining the return periods, it is necessary to calculate the cumulative frequency for every combination of values C_i- D_i. This is done with the aid of another VBA macro that calculates the cumulative frequency (CF_i) associated with every accumulated rainfall value, which is based on Partial Duration Series (PDS) analysis (Cunnane 1973) following the method in Palenzuela et al. (2016). More specifically, this analysis consist of the calculation of the observed cumulative frequency (CF ($X \leq x$)) for every recorded data instead of being restricted to longer prescribed durations (e.g., monthly or annual flows). The latter would apply to phenomena such as flooding or temperature peaks, where the Annual Maximum Series (AMS) or series of Maximum Annual Flows (MAF) are used. To calculate CF_i first the Weibull distribution (Weibull 1939) was applied to every C_i (Eq. 1) of the time series. However, this values are then converted to annual values through a factor *k* (Eq. 2)

$$CF_i = \frac{j}{N+1} \qquad \text{Eq. 1}$$

$$F_A = k \cdot \frac{j}{N+1} = \frac{No.days + 1}{No.years} \cdot \frac{No.ocurrences\ of\ X \leq x}{No\ days+1} = \frac{N+1}{Y} \cdot \frac{j}{N+1} = \frac{j}{Y} \quad \text{Eq. 2}$$

Where:

- Y represents the rainfall record length in years,
- N represents the number of data of the time series, in this case, equal to the number of days of the rainfall record, and
- *j* represents the number of occurrences of $X \leq x$, being X the variable C_i

Thus, through a PDS analysis CF_i is obtained for all the pairs of D_i-C_i values.

3) A third VBA macro automatically searches and tabulates the pairs of D_i-C_i values associated with every date in which landslide were triggered, and then calculates their mean intensity (I_i) and return period ($T_i = 1 / CF_i$). The mean intensity here is calculated as the amount of rainfall divided by the duration the rainfall event in days (I_i=C_i/D_i). Therefore, from this step, a table containing all the possible rainfall events with their parameters and return periods linked to past landslides is created. Considering the original database, 93 critical rainfall events were associated with the 93 dates in which the 153 landslides were registered. Furthermore, by varying the rainfall event duration, there are 90 possible rainfall events for every date. In total, there are 8370 possible rainfall events (93 dates x 90 durations) associated to the dated landslides. Accordingly, the following steps are focusing in extracting the most representative case of the critical rainfall for each of the 93 dates.

Figure 6. Flow diagram for the methodology

4) Once the necessary values were extracted, they were summarized by calculating the basic descriptive statistics (minimum, mean and maximum values) for D_i, C_i, I_i and T_i for every date associated with landslide events. The result for each statistic is stored in a table with 93 rows.
5) With the aim of determining the rainfall variable that better explain substantial changes in T, the bivariate correlation between rainfall variables (D_i, C_i or I_i) and the maximum return periods (T max.) for each of the 93 dates associated to landslides was studied through the Pearson correlation coefficient (r). In addition, graphs were built enabling the visual comparison of T peaks against rainfall variables peaks. After determining the rainfall variable that better explain T changes, a new search of rainfall parameters and return periods associated with the highest (maximum) values of that variable was run. Hence, a new dataset with 93 rows was generated. This dataset contains values of rainfall variables and return periods characterizing the critical rainfall events that can trigger one or more landslide when exceeded.

6) Once the 93 critical rainfall events are tabulated they are randomly divided into two datasets. The first dataset is used to generate CRT curves by using two rainfall parameters. The plotted points are then bounded by using a semiautomatic method to select and extract upper and lower points with the aid of a VBA macro, and then adjusting a power law function to every set of points. Although this method is more subjective when compared with statistic or probabilistic approaches (Brunetti et al 2010; Berti et al., 2012), it was used here because its easy and direct application to a point cloud. Thus, the upper curve will represent the more extreme conditions of the rainfall events that triggered landslides, while the lower curve will represent the curve of the lower (minimum) CRTs. In addition, more conservative curves are added when decreasing the lower CRT values in percentage steps. The second dataset was used to validate the performance of the CRT curves by showing the number of true positives (events that can trigger a landslide falling above the CRT curve) and false negatives (events that can trigger a landslide falling below the CRT curve).
7) As above mentioned, in this research the comparison between the return period of important rainfall event causing landslides and the recurrence of detected climatic cycles was carried out. This comparison will help to explain how climatic phenomena can increase landslides processes. To this end, a spectral analysis was applied, since it is a powerful statistical tool to analyse the distribution (over frequency) of the power contained in a signal, based on a finite dataset (Jenkins and Watts 1968; Pardo-Igúzquiza and Rodríguez-Tovar 2004; 2012). The processing of meteorological data using this technique seeks to determine the existence and statistical significance of climatic cycles (Knippertz 2003; Luque-Espinar et al. 2008; Karagiannidis et al. 2012). The calculations are based on the Blackman–Tukey approach (Blackman and Tukey 1958), which is known to be used to infer the power spectrum because it offers better results since the climatic cycles are well identified, and the statistical confidence is greater (Luque-Espinar et al. 2008; Pardo-Igúzquiza and Rodríguez-Tovar 2004; Pardo-Igúzquiza and Rodríguez-Tovar 2012).

The spectral analysis was performed by using the software POWGRAF2, and it fundamentals are found in Pardo-Igúzquiza and Rodríguez-Tovar (2004) and Blackman and Tukey (1958). In this context, a cycle has a very clear physical and mathematical meaning and is not a mere repetition of a hydrological property (Schwarzacher 2000) and can be represented by periodic function $f(t) = f(t + T)$, where T is the period. In this case, the spectrum analysis provides an adequate quantitative method to separate periodicities from signal noise in a data series. In the frequency domain, as studied in this case, the hydrological time series is represented as a sum of sinusoids with different amplitudes, phases and frequencies. In addition, hydrological time series are characterized by a finite number of data - N- and a constant temporal distance - Δ- between data. The spectral representation is then band limited between the frequency range

1/(NΔ) (Rayleigh frequency) and *1/(2*Δ*)* the Nyquist frequency (Pardo-Igúzquiza and Rodríguez-Tovar 2004).

The power spectrum (Pardo-Igúzquiza and Rodríguez-Tovar 2004) is calculated from the covariance function (Chatfield 1991) by:

$$\hat{S}(\omega) = \frac{1}{\pi}\left\{\lambda(0)\hat{C}(0) + \sum_{k=1}^{M}\lambda(k)\hat{C}(k)\cos(\omega k)\right\} \quad \text{Eq. 3}$$

Where $\hat{S}(\omega)$: estimated power spectrum for frequency ω.

$\hat{C}(k)$: estimated covariance function for the *k*-th lag.

cos(.): cosine

$\lambda(k)$: weighting function, known a lag-window, which is used to give less weight to the covariance estimates as the lag increases. For large lags, the estimated covariance function is less reliable. The lag-window used was the Tukey window (Tukey 1967):

$$\lambda(k) = \frac{1}{2}\left\{1 + \cos\left(\frac{\pi k}{M}\right)\right\} \; 0 \le k \le M \quad \text{Eq. 4}$$

M: maximum number of lags for the covariance function used in the spectral estimation. The maximum number of lags is *N-1*, with *N* being the number of experimental data; however, with large values for *M* a great number of peaks will be seen in the estimated power spectrum, most representing spurious cycles. On the other hand, if *M* is very small, significant cycles will not be seen in the estimated power spectrum. For this reason in this research the value of *M = N/2* was used in order to resolve peaks, and a value of *M=N/4* to determine the most significant peaks.

In addition to using a small value for *N*, confidence levels were estimated for the inferred power spectrum. The approach to estimate the confidence levels consists of fitting a background power spectrum with no cyclic component, but rather a smooth continuous spectrum, which is done by fitting the spectrum of an autoregressive process of order one, i.e. AR(1). The parameter of this process is estimated from the experimental data. We then take into account the known result for the one-sided confidence band of the power spectrum estimator used in the methodology proposed by Pardo-Igúzquiza and Rodríguez-Tovar 2004:

$$\mathrm{P}\left(\upsilon\frac{\hat{S}(\omega)}{S(\omega)} < \chi^2_{\upsilon,\alpha}\right) = 1-\alpha \quad \text{Eq. 5}$$

Where *P(.)*: probability operator.

$\hat{S}(\omega)$: Power spectrum estimate for frequency ω.

$S(\omega)$: Underlying power spectrum for frequency ω.

υ : Number of degrees of freedom. For the Blackman-Tukey estimate with a Tukey lag-window, the number of degrees of freedom is *2.67N/M.*

$\chi^2_{\upsilon,\alpha}$ Is the α quantile of a chi-square distribution with υ degrees of freedom.

α : Significance level.

For this study, we established confidence levels (CL) of 90%, 95% and 99%.

Once the climate cycles are detected their recurrence periods were compared with the highest return periods (> 1 y) of rainfall events that caused landslides.

5. Results

By means of the previous methodology, for each date in which one or more landslides were registered, 90 possible combinations of accumulated rainfall and mean intensity were obtained by taking into account 90 different durations. The integration of these 90 combinations with 93 dates of landslide occurrences resulted in 8370 different cases of rainfall variables values related to dated landslides. Then, the descriptive statistics of T-values (minimum, average and maximum) for every dated landslide, were obtained to be plotted (Figure 7) and visually compared with the rainfall parameters. Table 3 show the values of the maximum return period and rainfall parameters (Duration, Accumulated rainfall and Mean intensity for every date linked to the occurrence of landslides. Every rainfall event was identified with a unique ID. Accordingly, the rainfall duration (Fig. 8a), accumulated rainfall (Fig. 8b) and mean intensity (Fig. 8c) were plotted against the maximum return periods (representing the critical rainfall events). As seen from Fig. 7, the minimum and mean return periods of the landslide occurrences are less than one year. However, 24% of the landslides show maximum return periods longer than one year (Table 4). In general, from the PDS results, it could be observed that the greatest return periods are better correlated with the mean intensity (r = 0,36 in Table 5).

Table 4. Dates for the 22 rainfall events experiencing the greatest associated return period

Table 5. Pearson correlation coefficient (r) between pluviometric variables (duration, accumulated rainfall and mean intensity) and T max

In addition, the similarity between the peak patterns of the maximum return periods and the maximum mean intensity is graphically shown in Fig. 8c. However, no clear trend could be found, as shown by the scatter plot in Fig. 8d, preventing a reliable mathematical relationship between both variables. On the contrary, the remaining combinations showed common rainfall, with short to very short recurrence rates, and coinciding with periods of non-existing landslide record. Accordingly, the maximum mean intensity was selected to extract the rainfall parameters and return periods representing CRTs. The logical relationship between accumulated rainfall and duration has also been demonstrated (r = 0.87 in Table 5): longer duration rainfall events yield higher amounts of accumulated rainfall.

Table 3. Tabulated rainfall events. ID: rainfall event identifier; T max.: maximum return period; Dur.: duration; Accum. rainfall: accumulated rainfall; Mean int.: Mean intensity; # landslides: number of landslides

Figure 7. Plotting of the minimum, mean and maximum return period (T min, T mean and T max, respectively) for the cumulative rainfall corresponding with different durations for the 93 rainfall events associated with the catalogued landslides (left vertical axis). Readings on the right vertical axis show the number of landslides recorded for each case.

Figure 8. a) T max versus the duration of the linked rainfall events. b) T max versus the cumulative rainfall for the same events. c) T max versus mean intensity of such events. d) T max versus the corresponding mean intensity

It is worth noting that the cases with IDs: 12, 28, 60-63 and 81-87 display anomalous long return periods that match considerable increases in the number of registered landslides. However, in the other cases with similar increments in the occurrence of landslides, the return periods are not especially long. This effect is possibly related to the lack of information that characterizes the historic records (Ibsen and Brunsden 1996; Palenzuela et al. 2016).

As above mentioned, landslides are linked to the highest intensities when trying until 90 durations (from 1 day, by considering only the landslide date, to 90 days backward from this date) for every landslide date. Thus, the precipitation parameters and return periods referred to the maximum mean intensity were extracted to define the critical rainfall that can trigger one or more landslides in the study area.

The cumulative rainfall and duration for the critical rainfall events were randomly divided into two datasets. The first dataset containing 50 events was used to generate CRTs (Fig. 9) while the second dataset containing 43 events was used to test the performance of the CRT curves (Fig. 10). The lower CRT curve was adjusted to a group of lower points that were selected, and represents the cumulative rainfall (C) as a function of the rainfall duration (D). This CRT represents a first approximation for the estimation of rainfall thresholds values. However, after the validation phase, more conservative CRT curves were drawn by tentatively subtracting different percentages from these values (i.e.: C – (C x %C). By the same process, the upper bound was added showing the conditions (C-D) in which a rainfall event will surely trigger one or more landslides. Upper bound and lower curves were adjusted by using power law functions in the form: C = $\alpha\ D^{\beta}$, where α is a scaling constant (the intercept), and β is the shape parameter that defines the slope of the power law curve.

In this research the following functions were obtained to represent the upper bound and lower CRT curves with high correlation coefficients:

- Upper bound: C = $50.64D^{0.51}$, $R^2 = 0.97$ Eq. 6
- Lower limit: C = $6.85D^{0.51}$, $R^2 = 0.98$ Eq. 7

The lower CRT curve (lower limit) was validated observing some false negatives (rainfall events triggering landslides but falling below the lower limit), so different percentages (5%, 10%, …, 25%) were applied to decrease the values given by Eq. 7. Figures 9-10 show CRT curves for a subtraction of 10% and 25%, represented by Eqs. 8 and 9, respectively:

- 10% of the lower limit: C = $6.17D^{0.83}$ Eq. 8
- 25% of the lower limit: C = $5.14D^{0.83}$ Eq. 9

From the above equations it can be deduced an α parameter a 13% lower for the lower CRT curve than for the upper bound, while the β parameter remains constant. However, when considering the more conservative CRT curve (25%) a small change appears in α (from 6,85 to 5,14) while β increases in a 62 % (from 0,51 to 0,83).

From Figure 10 it can be observed that 4 critical rainfall events that triggered landslides fall below the curve representing the 10% of the lower CRT values. In other words, 4 of 43 events (10%) are still being considering as false negatives (FN). However, when using the curve representing the 25% of the lower CRT values, no events are placed below this curve. So this function it is selected here as the best one defining rainfall events that can trigger landslides for the study area.

Figure 9. Critical Rainfall Threshold curves. All dots represent duration and accumulated rainfall linked to the maximum mean intensity (peak) detected in the range from 1 to 90 duration days. Red dots were manual selected to fit the upper bound for critical rainfall events, whereas orange dots were selected to fit the lower critical rainfall threshold (lower limit) curve. CRT curves for the 10% and 25% of the lower limit are also represented

Figure 10. Plotting of the validation dataset. True positives (TP) are those rainfall events are plotted in zones above the lower limit, 10% of the lower limit or 25% of the lower limit, while false negatives (FN) are those events falling below these curves

The spectral analysis provides information about the climatic cycles, with different frequencies that may be related to well-known climatic phenomena. The detected cycles were as follows: semiannual, annual and Quasi-Biennial Oscillation (QBO) cycles above the 99% confidence level, and El Niño Southern Oscillation (ENSO), North Atlantic Oscillation (NAO) and solar (SUNSPOT) cycles with confidence levels less than 90% (Fig. 11). The cycles associated with QBO, ENSO, NAO and SUNSPOT were 2-2.9, 5-6, 6-10 and 10.5-12 years, respectively (Labitzke et al. 1990; Lamb, 1977; Hurrell, 1995; Stuiver and Braziunas 1989). Considering these climatic cycles, some temporal correlations were established between the maximum return periods and these climatic phenomena. As shown in Table 6, three rainfall events with maximum return periods of 5-6 years coincide with ENSO cycles, six events with maximum return periods of approximately 2 years correspond to QBO cycles, and three cases that occurred during March 2015 show a maximum return period of 10.3 years, likely associated with SUNSPOT cycles. It is worth noting that ENSO cases may be confused with harmonic SUNSPOT cycles (Lamb, 1977). However, it is clear that, despite rainfall with minor return periods appearing in that month, the highest return period for rainfall ending 27-31 March 2015, corresponds to SUNSPOT cycles (≈ 10 y). It is important to emphasize that these events correspond to the events with the greatest number of recorded landslides (> 5 in Fig. 7).

Figure 11. Power spectra of the "La Argelia" historical rainfall record. Detected cycles are represented through peaks: NAO (North Atlantic Oscillation), solar cycle (SUNSPOT), El Niño Southern Oscillation (ENSO), Quasi-Biennial Oscillation (QBO), annual cycle (ANNUAL), semiannual cycle (DEMIANNUAL)

Table 6. Correspondence between some of the rainfall events that generated landslides with known climatic cycles: solar cycle (SUNSPOT), El Niño Southern Oscillation (ENSO) and Quasi-Biennial Oscillation (QBO)

6. Discussion and final considerations

The creation of a spatiotemporal database of landslides in Loja (Ecuador) has enabled analysing the main factor that triggered them in this area: rainfall events. This database consists of a catalogue of 167 landslides, of which 153 were dated. The latter were triggered by 93 rainfall events that occurred between 2006 and 2015, and an increase in dated events was observed since 2011, possibly due to the growing concern about the negative consequences of landslides. In absence of more precise data, provided by in-situ testing instruments or more frequent precipitation measures, the daily rainfall record was utilized in this experimental research. To analyse the peculiarities of meteorological events linked to landslides, Critical Rainfall Thresholds (CRTs) were estimated through the use of PDS analysis. This analysis enabled studying the precipitation and return periods, while not constraining the results to prefixed durations of the recorded rainfall. Instead, the applied methodology extracted information in terms of the rainfall mean intensity and return period for each landslide event for periods between 1 and 90 days. This information served to estimate

CRT curves that describe the conditions that can trigger future landslides in the study area if the climate and geomorphic setting remains unchanged. For the case study, a first CRT curve was adjusted by using a potential function. Nonetheless, in this approach, a partial error may result from the point selection to adjust the lower CRT curve, which represents a drawback to be considered when compared with other methods (e.g. statistic or probabilistic methods). Consequently, to take into account the overall error, a more conservative CRT curve representing the minimum expected conditions (i.e., a combination between duration and accumulated rainfall) for triggering landslides in the study. This was carried out by applying a decreasing of 25% to the values of the first CRT curve, proving that no false negatives are produced when a test dataset of rainfall variables is checked against the CRT curves.

The recurrence rate of the studied precipitation periods associated with landslide events was compared to climatic cycles. Contrary to expectations, this study did not find a significant correlation between the estimated return periods and known climatic cycles. The major causes preventing this correlation are that (1) events with shorter return periods have been repeated more frequently than expected from those return periods, (2) some return periods coincide with any climatic cycle but also with a harmonic from another climatic cycle, and (3) the temporal length of the landslide catalogue does not enable checking the cyclic repetition of events with high return periods. This part of the methodology is constrained by the difference between the lengths of the available datasets. Specifically, in this research the entire rainfall record (52 years) was used to detect the climate cycles through the spectral analysis. However, the comparison was strongly influenced by the shorter length of the landslide catalogue (2006-2015). Despite of these constraints, it was found that the maximum return periods calculated for the rainfall events of March 2015 (generally 10,4 y) coincided with the temporal recurrence expected for the SUNSPOT cycles (10,5-12 y). In addition, the highest return period of this cycle prevents it of being a harmonic for the remaining detected cycles. Nonetheless, it is clear that a landslide catalogue with a longer temporal interval is necessary to recognize, with greater certainty, the relationship between the climatic cycles and landslide triggering. Moreover, a more complete and spatially distributed precipitation record would facilitate the analysis of the climatic influence of the studied region on the landslide frequency.

Regarding the landslide hazard in Loja, the results show that 76% of rainfall periods that trigger landslides in the study area have return periods of less than a year, and they are concentrated from February to April. This reflects the high temporal frequency of these hazardous phenomena in the study area. One interesting finding is that the number of rainfall events that trigger landslides was incremented in the last years of the series: 2011, 2012, 2014 and 2015. Moreover, 2015 was the year with the highest number of landslides recorded and the rainfall events during this year shows return periods of approximately 10 years, with a maximum of 17.3 years. In general, the catalogued landslide events showed relative short recurrence rates, suggesting that Loja is exposed to a high landslide hazard. For this reason, the landslide risk assessment and management should be taken seriously in the city of Loja.

Acknowledgements

This research has been supported through a grant awarded by the Ministry of Higher Education, Science, Technology and Innovation (SENESCYT) under the scholarship program "Open Call 2012 Second Phase" of the government of Ecuador. Furthermore, the major analysis on rainfall and landslide datasets have been possible thanks to the data provided by the Ecuadorian National Meteorological and Hydrologic Institute (INAMHI) and the Ecuadorian Secretary for Risk Management (SNGR-Zone 7). J.P. Galve acknowledges funding by the Spanish Ministry of Economy and Competitiveness through the 'Juan de la Cierva' Programme.

References

Aleotti P, Chowdhury R (1999) Landslide hazard assessment: summary review and new perspectives. Bull Eng Geol Environ 58(1):21–44

Aristizábal E, Vélez JI, Martínez HE, Jaboyedoff M (2016) SHIA_Landslide: a distributed conceptual and physically based model to forecast the temporal and spatial occurrence of shallow landslides triggered by rainfall in tropical and mountainous basins. Landslides 13(3):497-517

Baum RL, Godt JW (2010) Early warning of rainfall-induced shallow landslides and debris flows in the USA. Landslides 7(3): 259–272. doi: 10.1007/s10346-009-0177-0

Berti M, Martina MLV, Franceschini S, Pignone S, Simoni A, Pizziolo M (2012) Probabilistic rainfall thresholds for landslide occurrence using a Bayesian approach. J Geophys Res **Earth** Surf 117 (F4), doi: 10.1029/2012jf002367

Blackman RB, Tukey JW (1958) The measurement of power spectra from the point of view of communications engineering. Bell System Technical Journal 37(1):185–282

Borga M, Dalla Fontana G, Cazorzi F (2002) Analysis of topographic and climatic control on rainfall triggered shallow landsliding using a quasi-dynamic wetness index. J Hydrol 268 (1–4):56–71. doi:10.1016/s0022-1694(02)00118-x

Brabb EE (1991) The world landslide problem. Episodes, 14 (1):52-61

Brenning A, Schwinn M, Muenchow J (2015) Landslide susceptibility near highways is increased by 1 order of magnitude in the Andes of southern Ecuador, Loja province. Natural Hazards and Earth System Sciences 15(1):45-57

Brunetti, MT, Peruccacci, S, Rossi, M, Luciani, S, Valigi, D, & Guzzetti, F (2010) Rainfall thresholds for the possible occurrence of landslides in Italy. Nat Hazard Earth Sys 10(3):447-458. doi:10.5194/nhess-10-447-2010

Bussmann RW, Wilcke W, Richter M (2008) Landslides as important disturbance regimes—causes and regeneration. In Gradients in a tropical mountain ecosystem of Ecuador. Springer, Berlin Heidelberg, pp 319-330

Caine, N (1980) The rainfall intensity-duration control of shallow landslides and debris flows. Geografiska Annaler Series A 62(1-2): 23-27

Cadier E, Zevallos O, Basabe P (1996) El deslizamiento y las inundaciones catastroficas de la Josefina en el Ecuador. Bulletill de L´lnstitut Francais D'Etudes Andines 5(3):421-441

Cardinali M, Reichenbach P, Guzzetti F, Ardizzone F, Antonini G, Galli M, Cacciano M, Castellani M, Salvati P (2002) A geomorphological approach to the estimation of landslide hazards and risks in Umbria, Central Italy. Nat Hazard Earth Syst Sci 2(1–2):57–72doi:10.5194/nhess-2-57-200

Casale R, Fantecchi R, Flageolet JC (1994) Temporal occurrence and forecasting of landslides in the European Community. In: Casale R, Fantecchi R, Flageolet JC (eds) Final report. Programme Epoch (Ct. 90 0025). European Community, p 957

Chatfield, C., 1991. The Analysis of Time Series, fourth ed. Chapman and Hall, London, p. 241

Chacón J, Irigaray C, Fernández T, El Hamdouni R (2006) Engineering geology maps: landslides and geographical information systems. Bull Eng Geol Environ 65(4): 341-411. doi: 10.1007/s10064-006-0064-z

Corominas J., Moya J. (2008) A review of assessing landslide frequency for hazard zoning purposes. Eng Geol 102(3-4): 193-213. doi: 10.1016/j.enggeo.2008.03.018

Crozier M (1986) Landslides: causes, consequences and environment. Croom Helm, London, p 252

Crozier MJ, Eyles RJ (1980) Assessing the probability of rapid mass movement. In Proceedings of 3rd Australia-New Zealand Conference on Geomechanics, Wellington, N.Z.: Institution of Professional Engineers New Zealand, 1980: 2-47-2-51. Proceedings of Technical Groups. Vol. 6, p. 247-251

Cruden DM, Varnes DJ (1996) Landslide types and processes. In: Turner AK, Schuster RL (Eds) Landslides: investigation and mitigation. Sp. Rep. 247, Transportation Research Board, National Research Council. National Academy Press, Washington DC, pp 36–75

Cunnane C (1973) A particular comparison of annual maxima and partial duration series methods of flood frequency prediction. J Hydrol 18(3–4):257–271. doi:10.1016/0022-1694(73)90051-6

De Vita P, Napolitano E, Godt J, Baum R (2013) Deterministic estimation of hydrological thresholds for shallow landslide initiation and slope stability models: case study from the Somma-Vesuvius area of southern Italy. Landslides 10(6):713–728. doi:10.1007/s10346-012-0348-2

Dikau R, Cavallin A, Ja¨ger S (1996) Databases and GIS for landslide research in Europe. Geomorphology 15(3):227–239

Eras M (2014) Determinación de zonas susceptibles a movimientos en masa en el Ecuador, a escala 1:1.000.000 utilizando el método de ponderación de parámetros. Tesis de pregrado. Escuela Politécnica Nacional. Quito, Ecuador, p 119

Frattini P, Crosta GB, Fusi N, Dal Negro P (2004) Shallow landslides in pyroclastic soils: A distributed modelling approach for hazard assessment. Eng Geol 73(3–4):277–295. doi:10.1016/j.enggeo.2004.01.009

Gariano SL, Brunetti MT, Iovine G, Melillo M, Peruccacci S, Terranova O, Vennari C, Guzzetti F (2015). Calibration and validation of rainfall thresholds for shallow landslide forecasting in Sicily, Southern Italy. Geomorphology 228: 653-665. doi: 10.1016/j.geomorph.2014.10.019

Gariano SL, Guzzetti F (2016) Landslides in a changing climate. Earth-Science Reviews 162: 227-252. doi: dx.doi.org/10.1016/j.earscirev.2016.08.011

Glade T, Crozier M, Smith P (2000) Applying probability determination to refine landslide-triggering rainfall thresholds using an empirical ‘‘Antecedent Daily Rainfall Model’’. Pure appl Geophys 157(6–8):1059–1079. doi:10.1007/s000240050017

González Garcia AJ, Mayorga Marquez R (2004) Thresholds for rainfall events that induce landslides in Colombia. Landslides: Evaluation and Stabilization, Taylor and Francis Group, London, pp 349-355

Guzzetti F, Carrara A, Cardinali M, Reichenbach P (1999) Landslide hazard evaluation: a review of current techniques and their application in a multi-scale study, Central Italy. Geomorphology 31(1–4):181–216. doi:10.1016/S0169-555X(99)00078-1

Guzzetti F, Peruccacci S, Rossi M, Stark CP (2007) Rainfall thresholds for the initiation of landslides in central and southern Europe. Meteorol Atmos Phys 98(3–4):239–267. doi:10.1007/s00703-007-0262-7

Guzzetti F, Peruccacci S, Rossi M, Stark C (2008) The rainfall intensity–duration control of shallow landslides and debris flows: an update. Landslides 5(1):3–17. doi:10.1007/s10346-007-0112-1

Haque CE, Burton I (2005) Adaptation Options Strategies for Hazards and Vulnerability Mitigation: An International Perspective. Mitig adapt strategies glob Chang 10 (3): 335-353. doi: 10.1007/s11027-005-0050-y

Henn B, Cao Q, Lettenmaier DP, Magirl CS, Mass C, Bower JB, Laurent MS, Mao Y, Perica S (2015) Hydroclimatic Conditions Preceding the March 2014 Oso Landslide. J Hydrol 16(3):1243-1249. doi: 10.1175/jhm-d-15-0008.1

Hermanns RL, Valderrama P, Fauqué L, Penna IM, Sepúlveda S, Moreiras S, Zavala Carrión B (2012) Landslides in the Andes and the need to communicate on an interandean level on landslide mapping and research. Rev Asoc Geol Argent 69(3):321-327

Hungerbühler D, Steinmann M, Winkler W, Sewards D, Egüez A, Peterson DE, Helg U, Hammer C (2002) Neogene stratigraphy and Andean geodynamics of southern Ecuador. Earth-Science Rev 57:75–124. doi: 10.1016/S0012-8252(01)00071-X

Hung C, Lin GW, Syu HS, Chen CW, Yen HY (2017) Analysis of the Aso-Bridge landslide during the 2016 Kumamoto earthquakes in Japan. Bull Eng Geol Env. doi: 10.1007/s10064-017-1103-7

Hurrell JW (1995) Decadal trends in the North Atlantic Oscillation: regional temperatures and precipitation. Science 269(5224):676-679

Ibadango C, Soto J, Tamay J, Escudero P, Porter M (2005) Mass movements in the Loja Basin-Ecuador, South America. Proceedings, Int Conf Landslide Risk Management. Vancouver, Canada 10:1-7

Ibsen ML, Brunsden D (1996) The nature, use and problems of historical archives for the temporal occurrence of landslides, with specific reference to the south coast of Britain, Ventnor. Isle of Wight. Geomorphology 15(3–4):241–258. doi:10.1016/0169-555X(95)00073-E

INEC (2010) Instituto Nacional de Estadísticas y Censos. VII Censo de población y VI de vivienda. Ecuador. URL: http://www.inec.gob.ec

INIGEMM (2013) Instituto Nacional de Investigación Geológico Minero y Metalúrgico. Mapa de susceptibilidad por movimientos en masa del Ecuador, escala 1:1,000,000. Technical report. Unpublished

Jenkins GM, Watts DG (1968) Spectral analysis and its applications. Holden-Day, San Francisco, p 525

Karagiannidis AF, Karacostas T, Maheras P, Makrogiannis T (2012) Climatological aspects of extreme precipitation in Europe, related to mid-latitude cyclonic systems. Theoretical and Applied Climatology 107(1-2):165-174

Kennerley JB (1980) Outline of the geology of Ecuador. Overseas Geology Mineral Resources 55:17

Kim SK, Hong WP, Kim YK (1991) Prediction of rainfall-triggered landslides in Korea. In: Bell C (ed) 6th international symposium on landslides, vol 2. A.A. Balkema, Rotterdam

Knippertz P (2003) Tropical-extratropical interactions causing precipitation in Northwest Africa: statistical analysis and seasonal variations. Monthly weather review, 131(12):3069-3076

Kumar A, Asthana A, Priyanka R S, Jayangondaperumal R, Gupta A D, Bhakuni SS (2017) Assessment of landslide hazards induced by extreme rainfall event in Jammu and Kashmir Himalaya, northwest India, Geomorphology 284: 72-87. doi: 10.1016/j.geomorph.2017.01.003

Labitzke K, Van Loon H, Shine K (1990) Associations between the 11-Year Solar Cycle, the Quasi-Biennial Oscillation and the Atmosphere: A Summary of Recent Work [and Discussion]. Philosophical Transactions of the Royal Society of London A: Mathematical, Physical and Engineering Sciences 330(1615):577-589

Lacasse S, Nadim F (2009) Landslide risk assessment and mitigation strategy. In: Sassa K, Canuti P (eds) Landslides—disaster risk reduction. Springer, Berlin, Sec. 3, p 31–61. ISBN/ISSN: 978-3-540-69966-8. doi:10.1007/978-3-540-69970-5_3

Lamb HH (1977) Climate history and the future. Methuen, London, p 212

Larsen MC, Wieczorek GF (2006) Geomorphic effects of large debris flows and flash floods, northern Venezuela, 1999. Z. Geomorph. NF suppl 145:147-175

Larsen MC (2008) Rainfall-triggered landslides, anthropogenic hazards, and mitigation strategies. Adv Geophys 14:147-153

Li C, Ma T, Zhu X, Li W (2011) The power-law relationship between landslide occurrence and rainfall level. Geomorphology 130(3–4):221–229. doi:10.1016/j.geomorph.2011.03.018

Litherland M, Aspden JA, Jemielita RA (1994) The metamorphic belts of Ecuador, British Geological Survey, Overseas Memoir 11. BGS, Keyworth, p 147

Lozano P, Bussmann RW, Küppers M (2005) Landslides as ecosystem disturbance—their implications and importance in South Ecuador. Lyonia 8(1):67-72

Lumb P (1975) Slope failure in Hong Kong. Q J Eng Geol 8:31–65

Luque-Espinar JA, Chica-Olmo M, Pardo-Igúzquiza E, García-Soldado MJ (2008) Influence of climatological cycles on hydraulic heads across a Spanish aquifer. J Hydrol 354(1):33-52

Marui H, Wanfg C (2015) Earthquake-Induced Landslides: An Overview. In: Lollino G, Giordan D, Crosta GB et al (eds) Engineering Geology for Society and Territory - Volume 2: Landslide

Processes. Springer International Publishing. ISBN/ISSN: 978-3-319-09057-3. doi: 10.1007/978-3-319-09057-3_119. pp 713-715

Ma T, Li C, Lu Z, Wang B (2014) An effective antecedent precipitation model derived from the power-law relationship between landslide occurrence and rainfall level. Geomorphology 216:187–192. doi:10.1016/j.geomorph.2014.03.033

Muenchow J, Brenning A, Richter M (2012) Geomorphic process rates of landslides along a humidity gradient in the tropical Andes. Geomorphology, 139:271-284

Nadim F, Kjekstad O, Peduzzi P, Herold C, Jaedicke C (2006) Global landslide and avalanche hotspots. Landslides 3(2): 159-173. doi: 10.1007/s10346-006-0036-1

Nikolopoulos EI, Crema S, Marchi L, Marra F, Guzzetti F, Borga M (2014) Impact of uncertainty in rainfall estimation on the identification of rainfall thresholds for debris flow occurrence. Geomorphology 221: 286-297. doi: 10.1016/j.geomorph.2014.06.015

Palenzuela JA, Jiménez-Perálvarez JD, Chacón J, Irigaray C (2016) Assessing critical rainfall thresholds for landslide triggering by generating additional information from a reduced database: an approach with examples from the Betic Cordillera (Spain). Nat Hazards 84 (1): 185-212. doi: 10.1007/s11069-016-2416-8

Panizza M (1996) 3 Geomorphological hazard. In: Mario P (eds) Developments in earth surface processes. Elsevier, vol 4, pp 75–76. ISBN/ISSN: 0928-2025. doi: 10.1016/S0928-2025(96)80020-4

Papa MN, Medina V, Ciervo F, Bateman A (2013) Derivation of critical rainfall thresholds for shallow landslides as a tool for debris flow early warning systems. Hydrol Earth Syst Sci 17(10):4095–4107. doi:10.5194/hess-17-4095-2013

Pardo-Igúzquiza E, Rodríguez-Tovar FJ (2012) POWGRAF2: a program for graphical spectral analysis in cyclostratigraphy. Computers & Geosciences 30 (2004) 533–542

Pardo-Igúzquiza E, Rodríguez-Tovar FJ (2012) Spectral and cross-spectral analysis of uneven time series with the smoothed Lomb–Scargle periodogram and Monte Carlo evaluation of statistical significance. Computers & Geosciences, 49:207-216

Petley D, Dunning SA, Rosser NJ (2005) The analysis of global landslide risk through the creation of a database of worldwide landslide fatalities. Landslide risk management. Balkema, Amsterdam, pp 367-374

Petley DN, Hearn GJ, Hart A, Rosser NJ, Dunning SA, Oven K, Mitchell WA (2007) Trends in landslide occurrence in Nepal. Nat Haz 43(1): 23-44. doi: 10.1007/s11069-006-9100-3

Petley D (2012) Global patterns of loss of life from landslides. Geology. The Geological Society of

America, vol 40. 10, pp 927–930. ISBN/ISSN: 0091-7613. doi: 10.1130/G33217.1

PNUMA M. D. L. Naturaleza y Cultura Internacional (2007) Perspectivas del Medio Ambiente Urbano GEO Loja. Loja, Ecuador.

PMA (2007) Proyecto Multinacional Andino: Geociencias para las Comunidades Andinas. Movimientos en masa en la Región Andina: Una guía para la evaluación de amenazas. Servicio Nacional de Geología y Minería, Publicación Geológica Multinacional, No. 4, p 432, 1 cd-rom

Rossi M, Peruccacci S, Guzzetti F (2006) A review of rainfall thresholds for the initiation of landslides. Geophys Res Abstr 8:02323

Runqiu H (2009) Some catastrophic landslides since the twentieth century in the southwest of China. Landslides 6(1): 69-81. doi: 10.1007/s10346-009-0142-y

Saito H, Nakayama D, Matsuyama H (2010) Relationship between the initiation of a shallow landslide and rainfall intensity-duration thresholds in Japan. Geomorphology 118, (1-2), 2010, Pages 167-175, ISSN 0169-555X, doi: 10.1016/j.geomorph.2009.12.016

Sassa K, Tsuchiya S, Fukuoka H, Mikos M, Doan L (2015) Landslides: review of achievements in the second 5-year period (2009–2013). Landslides (2):213-223. doi: 10.1007/s10346-015-0567-4

Segoni S, Rossi G, Rosi A, Catani F (2014) Landslides triggered by rainfall: A semi-automated procedure to define consistent intensity–duration thresholds. Comput Geos 63: 123-131. doi: http://dx.doi.org/10.1016/j.cageo.2013.10.009

Sepúlveda SA, Rebolledo S, Vargas G (2006) Recent catastrophic debris flows in Chile: Geological hazard, climatic relationships and human response. Quat Int 158(1):83-95

Schuster RL, Highland LM (2001) Socioeconomic and Environ-mental Impacts of Landslides in the Western Hemisphere. Open-File Report 01-0276, US Geological Survey, p. 47

Shanmugam G, Wang Y (2015) The landslide problem. J Palaeogeogr 4(2): 109-166. doi: dx.doi.org/10.3724/SP.J.1261.2015.00071

SNGR/ECHO/UNISDR (2012) Secretaría Nacional de Gestión de Riesgos. Ecuador: Referencias Básicas para la Gestión de Riesgos. Quito, Ecuador.

Stuiver M, Braziunas TF (1989) Atmospheric 14C and century-scale solar oscillations. Nat 388: 405-407

Song K, Wang F, Dai Z, Iio A, Osaka O, Sakata S (2017) Geological characteristics of landslides triggered by the 2016 Kumamoto earthquake in Mt. Aso volcano, Japan. Bull Eng Geol. doi: 10.1007/s10064-017-1097-1

Soto J, Galve JP, Palenzuela JA, Azañón JM, Tamay J, & Irigaray C (2017) A multi-method approach for the characterization of landslides in an intramontane basin in the Andes (Loja, Ecuador). Landslides, 1-19.

Schwarzacher W (2000) Repetitions and cycles in stratigraphy. Earth-Sci Rev 50 (1): 51-75. doi: dx.doi.org/10.1016/S0012-8252(99)00070-7

Terlien MTJ (1996) Modelling spatial and temporal variations in rainfall-triggered landslides: the integration of hydrologic models, slope stability models and geographic information systems for the hazard zonation of rainfall-triggered landslides with examples from Manizales (Colombia). International Institute for Aerial Survey and Earth Sciences (ITC).

Terlien MTJ (1997) Hydrological landslide triggering in ash-covered slopes of Manizales (Colombia). Geomorphology 20(1):165-175

Terlien MTJ (1998) The determination of statistical and deterministic hydrological landslide-triggering thresholds. Environ Geol 35(2–3):124–130. doi:10.1007/s002540050299

Tukey JW (1967) An introduction to the calculations of numerical spectrum analysis. In Harris B (ed) Spectral Analysis of Time Series, Wiley, New York, pp 25–46

UNESCO (1973–1979) Annual summaries of information on natural disasters, 1971–1975. UNESCO, Paris

Van Den Eeckhaut M, Herva´s J (2012) State of the art of national landslide databases in Europe and their potential for assessing landslide susceptibility, hazard and risk. Geomorphology 139–140:545–558. doi:10.1016/j.geomorph.2011.12.006

Weibull W (1939) A statistical theory of the strength of materials. Ing Velenskaps Akad Handl 151: 1-45

Xu XZ, Guo WZ, Liu YK, Ma JZ, Wang WL, Zhang HW, Gao H (2017) Landslides on the Loess Plateau of China: a latest statistics together with a close look. Nat Haz 86(3): 1393-1403. doi: 10.1007/s11069-016-2738-6

Zhuang, J, Peng, J, Wang, G, Iqbal, J, Wang, Y, Li, W, Xu, Q, Zhu, X (2017) Prediction of rainfall-induced shallow landslides in the Loess Plateau, Yan'an, China, using the TRIGRS model. Earth Surf. Process. Landforms 42: 915–927. doi: 10.1002/esp.4050

FIGURES AND FIGURE CAPTIONS

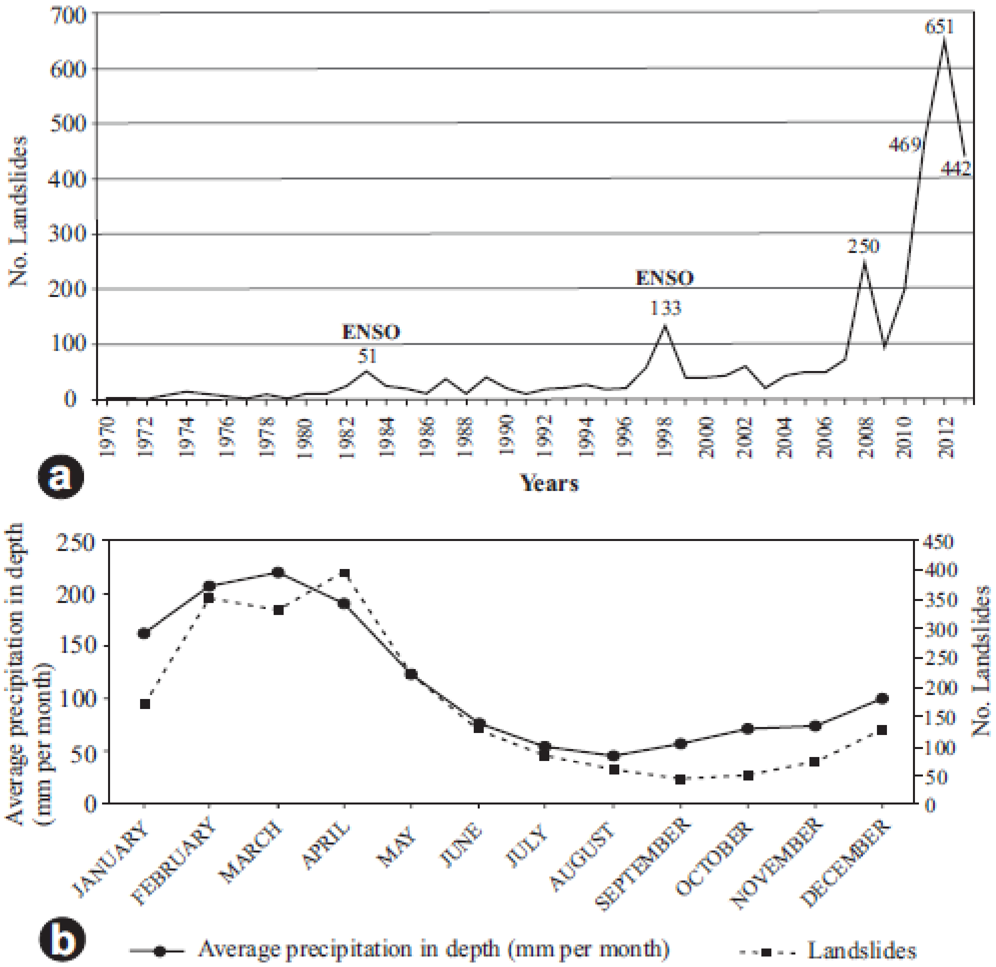

Figure 1. a) Annual distribution of landslides generated in Ecuador (1970 – 2013) showing El Niño–Southern Oscillation (ENSO) events; b) Relationship between the number of landslides and the mean monthly precipitation (1970 – 2011) (Eras, 2014).

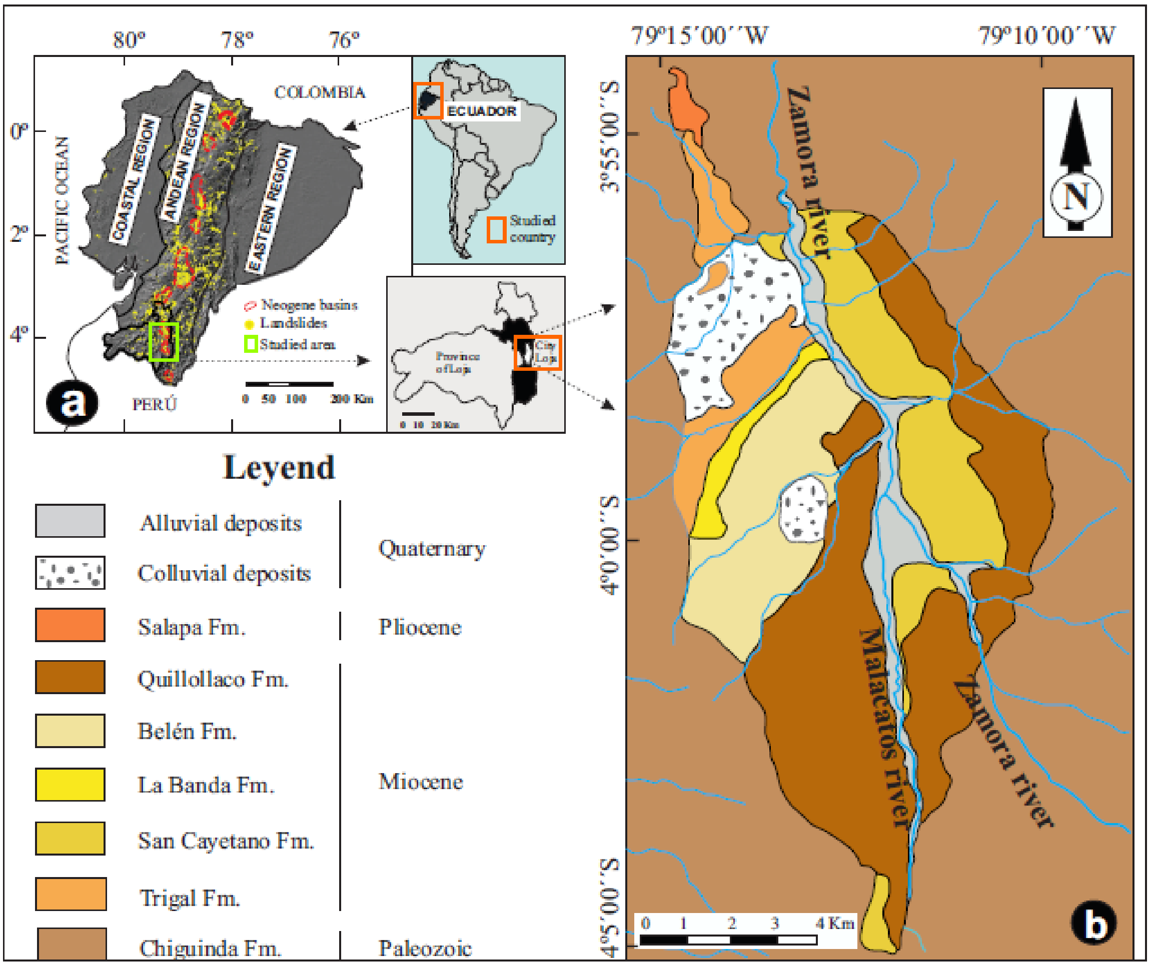

Figure 2. Geographical and geological setting of the study area: a) Ecuador regions and landslide inventory (INIGEMM, 2013); b) Geological formations of the study area.

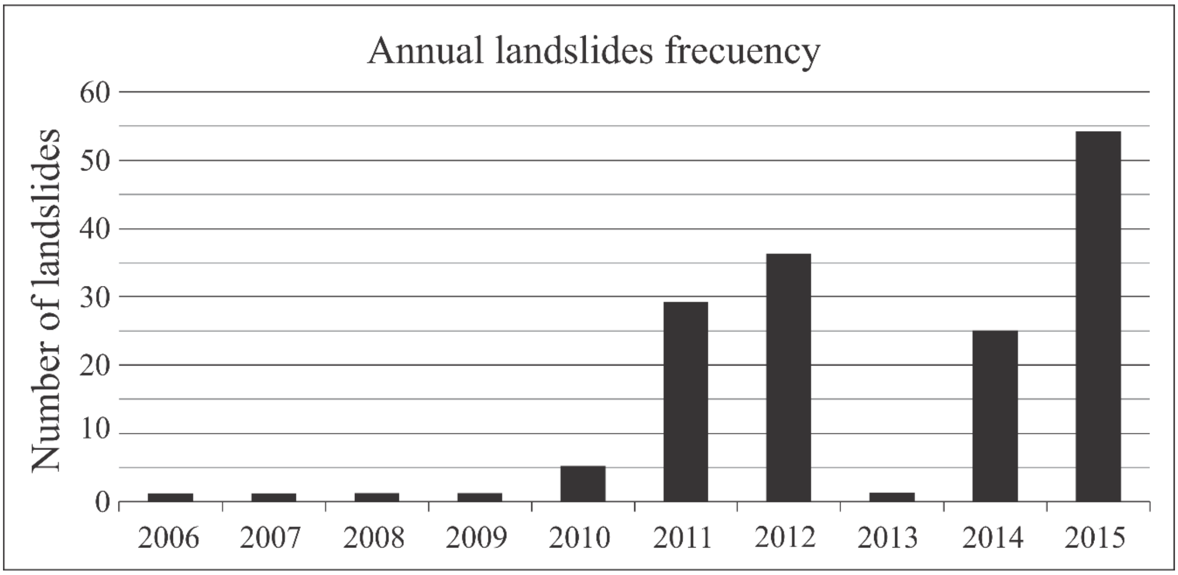

Figure 3. Annual distribution of landslides in Loja that occurred between 2006 and 2015

Trigger	Rainfall	Poor drainage	Excavation slope	Stream socavation	Unreported
Landsides	151	2	11	2	1

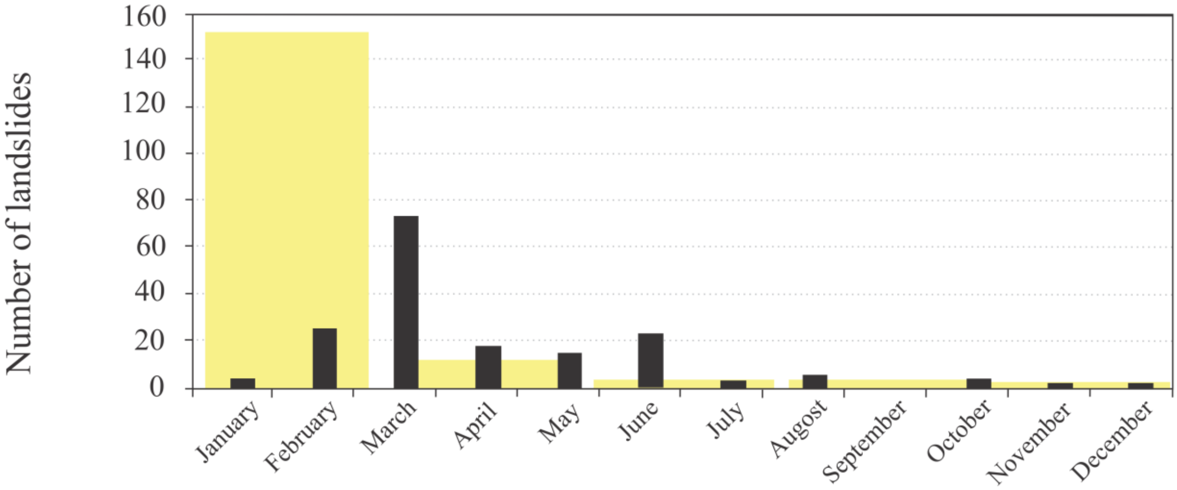

Landsides	3	25	74	17	14	22	2	5	---	3	1	1

Figure 4. Main triggers of landslides in southern Ecuador and monthly distribution of the catalogued landslides (2010 – 2015). Black bars represent the number of landslides by month, while yellow bars represent the number of landslides by trigger type

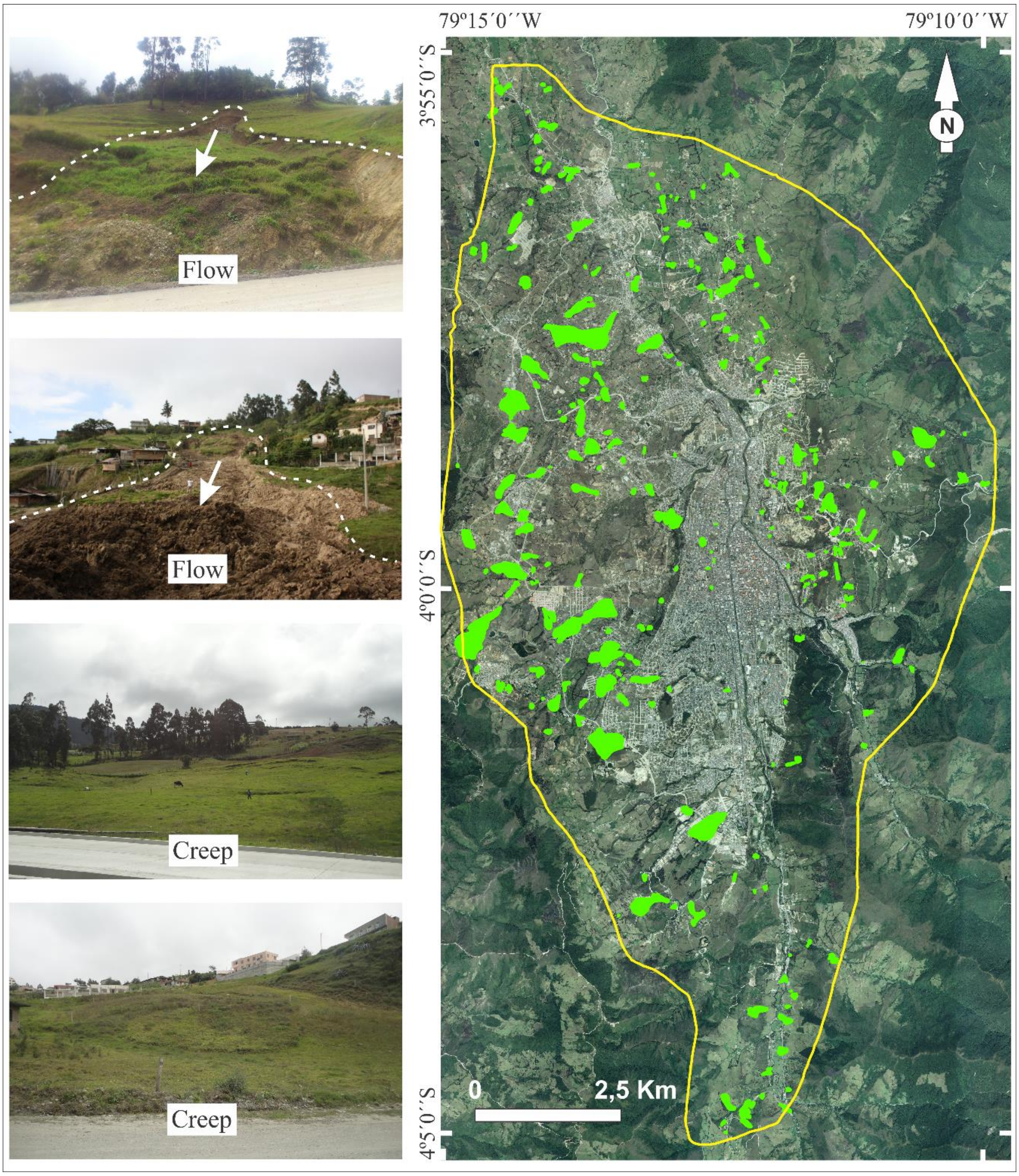

Figure 5. Landslide inventory in the study area (green polygons) and photographs of predominant types.

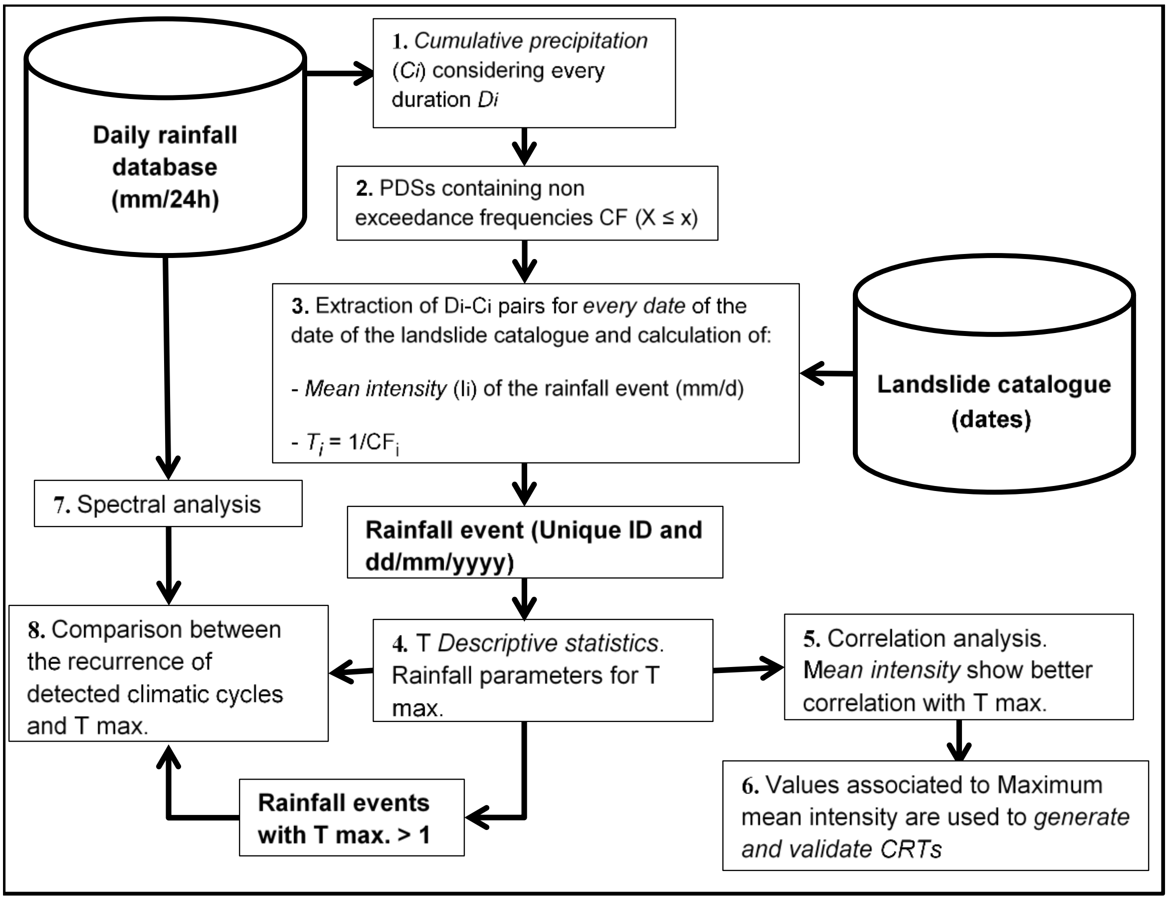

Figure 6. Flow diagram for the methodology

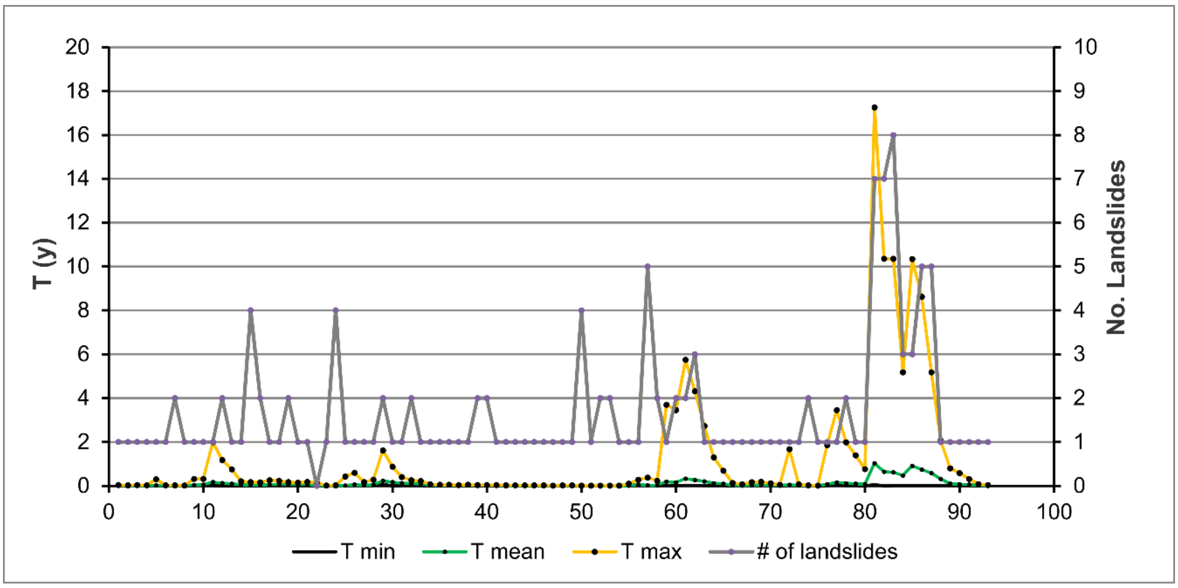

Figure 7. Plotting of the minimum, mean and maximum return period (T min, T mean and T max, respectively) for the cumulative rainfall corresponding with different durations for the 93 rainfall events associated with the catalogued landslides (left vertical axis). Readings on the right vertical axis show the number of landslides recorded for each case.

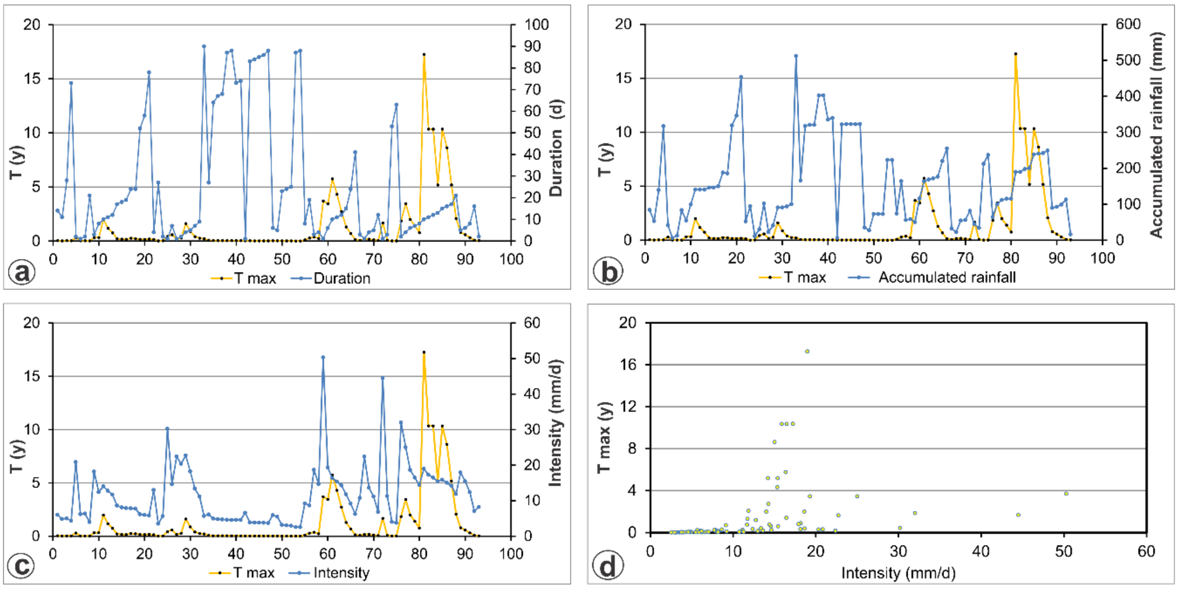

Figure 8. a) T max versus the duration of the linked rainfall events. b) T max versus the cumulative rainfall for the same events. c) T max versus mean intensity of such events. d) T max versus the corresponding mean intensity

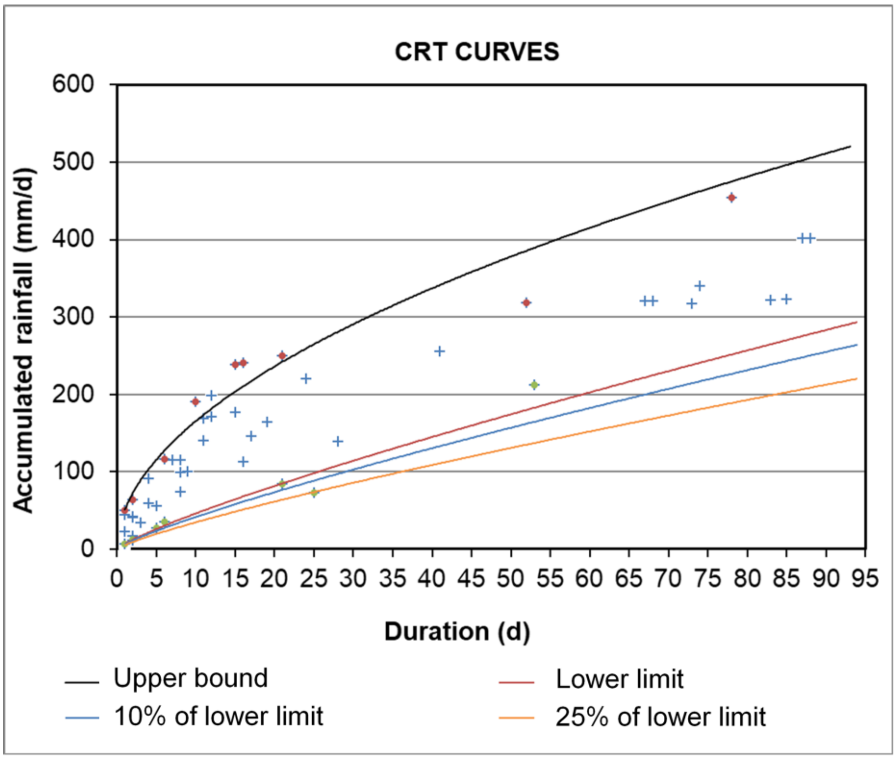

Figure 9. Critical Rainfall Threshold curves. All dots represent duration and accumulated rainfall linked to the maximum mean intensity (peak) detected in the range from 1 to 90 duration days. Red dots were manual selected to fit the upper bound for critical rainfall events, whereas orange dots were selected to fit the lower critical rainfall threshold (lower limit) curve. CRT curves for the 10% and 25% of the lower limit are also represented

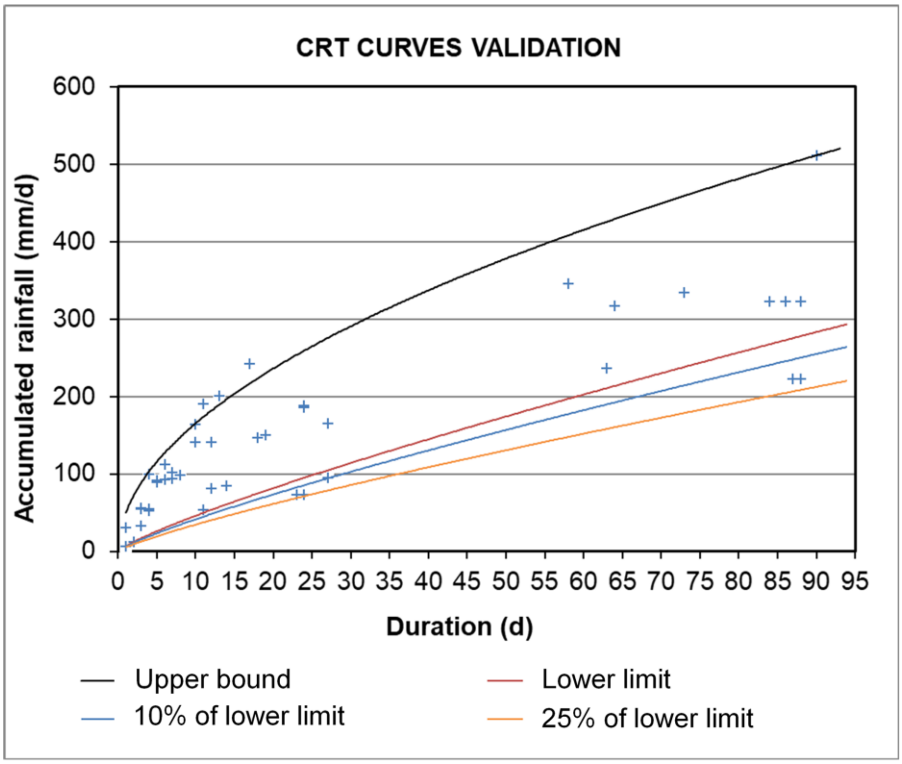

Figure 10. Plotting of the validation dataset. True positives (TP) are those rainfall events are plotted in zones above the lower limit, 10% of the lower limit or 25% of the lower limit, while false negatives (FN) are those events falling below these curves

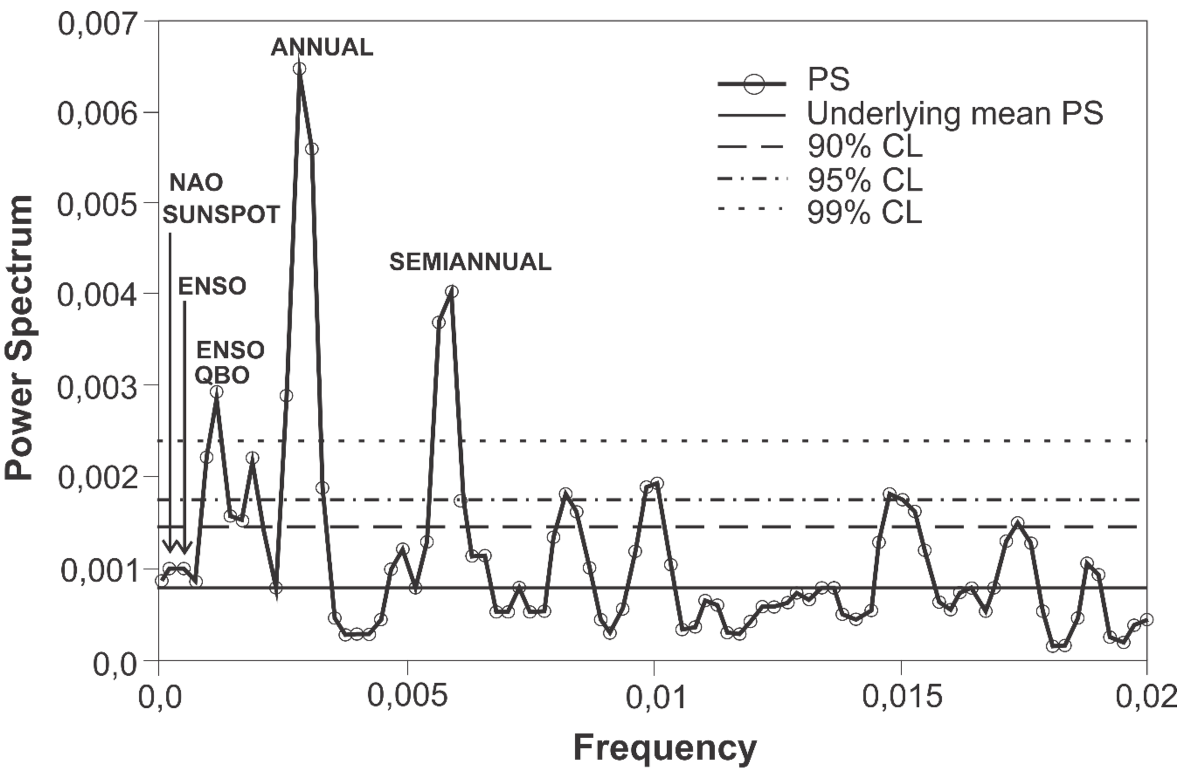

Figure 11. Power spectra of the "La Argelia" historical rainfall record. Detected cycles are represented through peaks: NAO (North Atlantic Oscillation), solar cycle (SUNSPOT), El Niño

Southern Oscillation (ENSO), Quasi-Biennial Oscillation (QBO), annual cycle (ANNUAL), semiannual cycle (DEMIANNUAL)

TABLES AND TABLE CAPTIONS

Table 1. Landslides with major damage caused in the Andean region, triggered by rainfall

Locality	Country	Year	Summary	Deaths	Damage Millon ($)	References
Vargas	Venezuela	1999	DebrisFlow	15000	4000	Salcedo en PMA 2007 Larsen & Wieczorek, 2006;
Río Limón (Aragua)	Venezuela	1987	Debrisflow	210	n/d	PMA 2007
Villatina	Colombia	1987	Earthflow	450	n/d	PMA 2007
Cerro Pucaloma (La Paz)	Bolivia	2003	Traslational	69	n/d	PMA 2007
Mayunmarca	Perú	1974	Traslational/flow	600	n/d	PMA 2007
Antofagasta	Argentina	1991	DebrisFlow	91	n/d	PMA 2007
Antofagasta Santiago Ranco Lake	Chile	1991 1993 2004	Debrisflows	130	71	Sepúlveda et al. 2006
Chunchi	Ecuador	1983	n/d	150	n/d	Petley et al. 2005
The Josefina	Ecuador	1993	Flow	35	147	Petley et al. 2005; Cadier et al. 1996; Zevallos et al. 1996

Table 2. Reported damage due to landslides in the Loja basin between 2010 and 2015 (SNGR – Zona 7)

Types of damage	Quantity	Approximate costs	Number of landslides
Affected people	1913		global
Deaths	7	unquantifiable	2
Destroyed houses	40	2000000	11
Partially affected housing	219	1095000	105
Affectation of the roads	620 meters		33
Affectation of water pipes	non reported		8
No affections reported			8
Total			**167**

Table 3. Tabulated rainfall events. ID: rainfall event identifier; T max.: maximum return period; Dur.: duration; Accum. rainfall: accumulated rainfall; Mean int.: Mean intensity; # landslides: number of landslides

ID	End date	T max. (y)	Dur. (d)	Accum. rainfall (mm)	Mean Int. (m/d)	# land-slides
81	26/03/2015	17.3	10	189.9	19.0	7
82	27/03/2015	10.4	11	189.9	17.3	7
83	28/03/2015	10.4	12	197.9	16.5	8

85	31/03/2015	10.3	15	238.5	15.9	3
--	--	--	--	--	--	--

Table 4. Dates for the 22 rainfall events experiencing the greatest associated return period

Date	T max. (y)	Date	T max. (y)
26/03/2015	17.3	05/03/2014	3.5
27/03/2015	10.4	11/03/2014	2.7
28/03/2015	10.4	06/04/2015	2.1
31/03/2015	10.3	22/03/2015	2.0
01/04/2015	8.6	15/02/2011	2.0
09/03/2014	5.8	18/03/2015	1.8
29/03/2015	5.2	25/10/2014	1.7
02/04/2015	5.2	28/02/2012	1.6
10/03/2014	4.3	23/03/2015	1.4
04/03/2014	3.7	14/03/2014	1.3
20/03/2015	3.5	16/02/2011	1.2

Table 5. Pearson correlation coefficient (r) between pluviometric variables (duration, accumulated rainfall and mean intensity) and T max

	T max.	Dur. (d)	Accum. rainfall (mm)	Mean int. (mm/d)
T max.	1.00			
Dur. (d)	-0.22	1.00		
Accum. rainfall (mm)	0.07	0.87	1.00	
Mean int. (mm/d)	**0.36**	-0.56	-0.41	1.00

Table 6. Correspondence between some of the rainfall events that generated landslides with known climatic cycles: solar cycle (SUNSPOT), El Niño Southern Oscillation (ENSO) and Quasi-Biennial Oscillation (QBO)

Event No.	Date	T max. (Y)	Corresponding cycle
11	15/02/2011	2.0	QBO
29	28/02/2012	1.6	QBO
61	09/03/2014	5.8	ENSO
63	11/03/2014	2.7	QBO
72	25/10/2014	1.7	QBO
76	18/03/2015	1.8	QBO
78	22/03/2015	2.0	QBO
82	27/03/2015	10.4	SUNSPOT
83	28/03/2015	10.4	SUNSPOT
84	29/03/2015	5.2	ENSO

85	31/03/2015	10.3	SUNSPOT
87	02/04/2015	5.2	ENSO
88	06/04/2015	2.1	QBO

Figure 1

Click here to download Figure Figure 1.tif

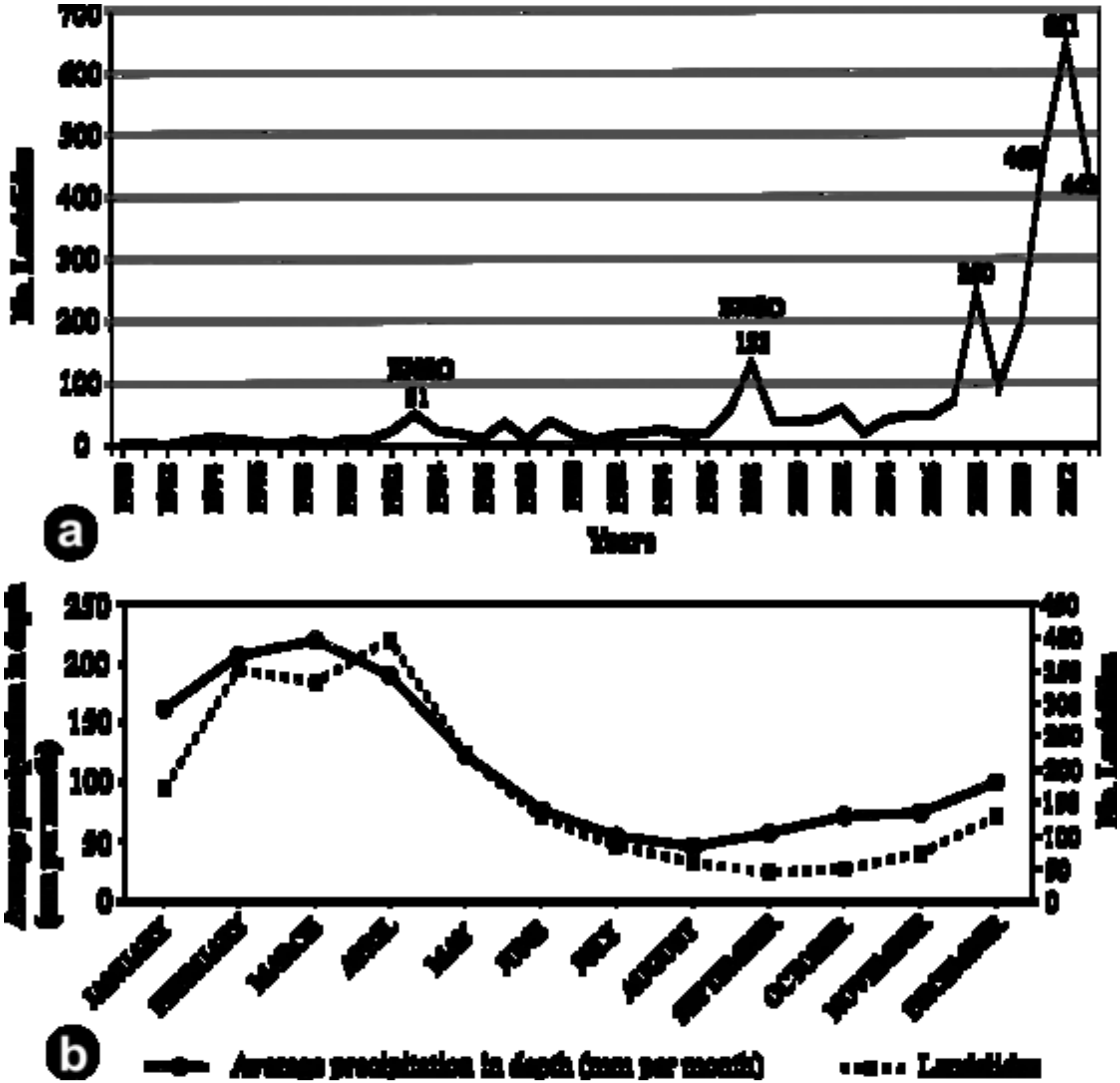

Figure 2 Click here to download Figure Figure 2.tif

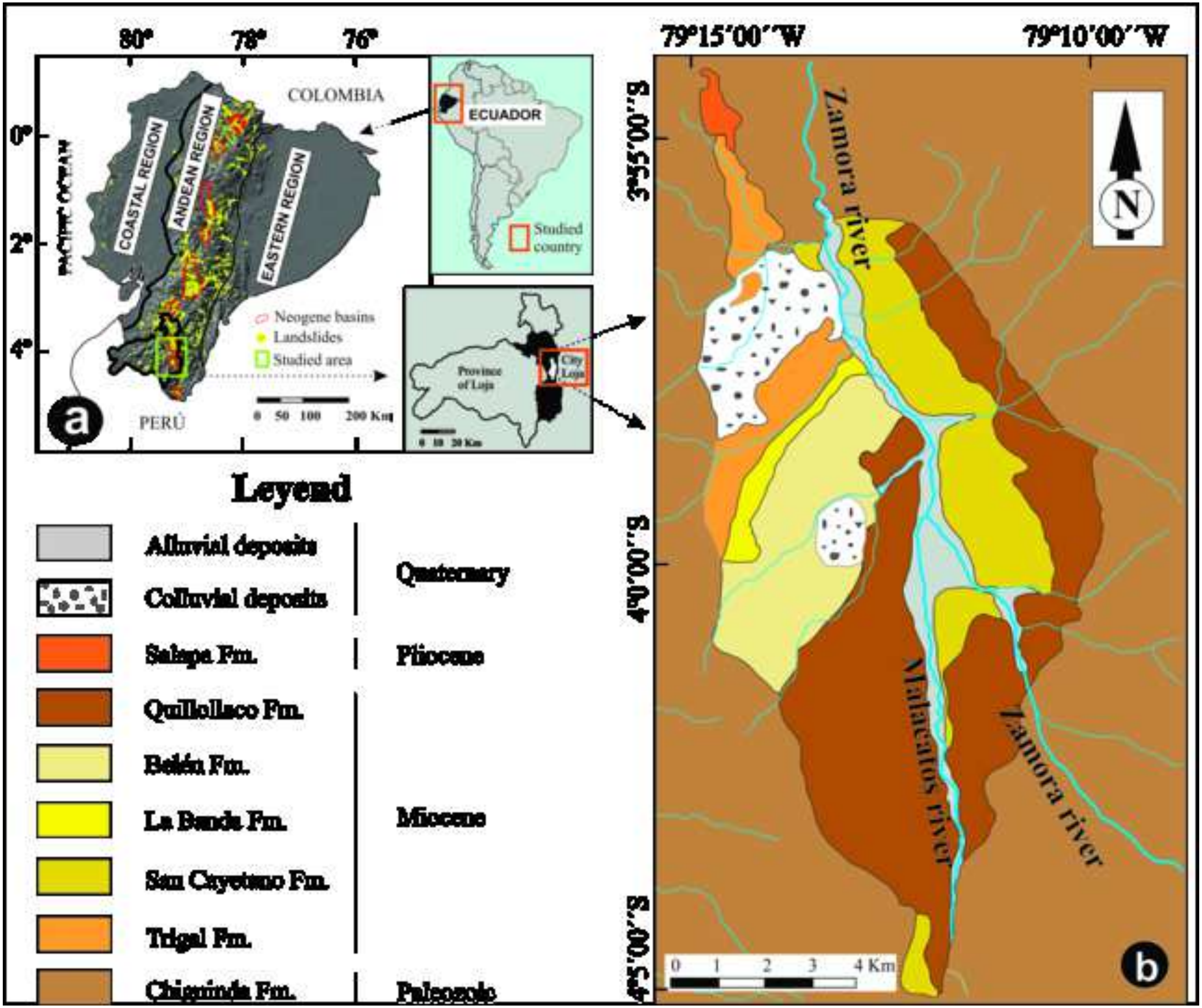

Figure 3

Click here to download Figure Figure 3.tif

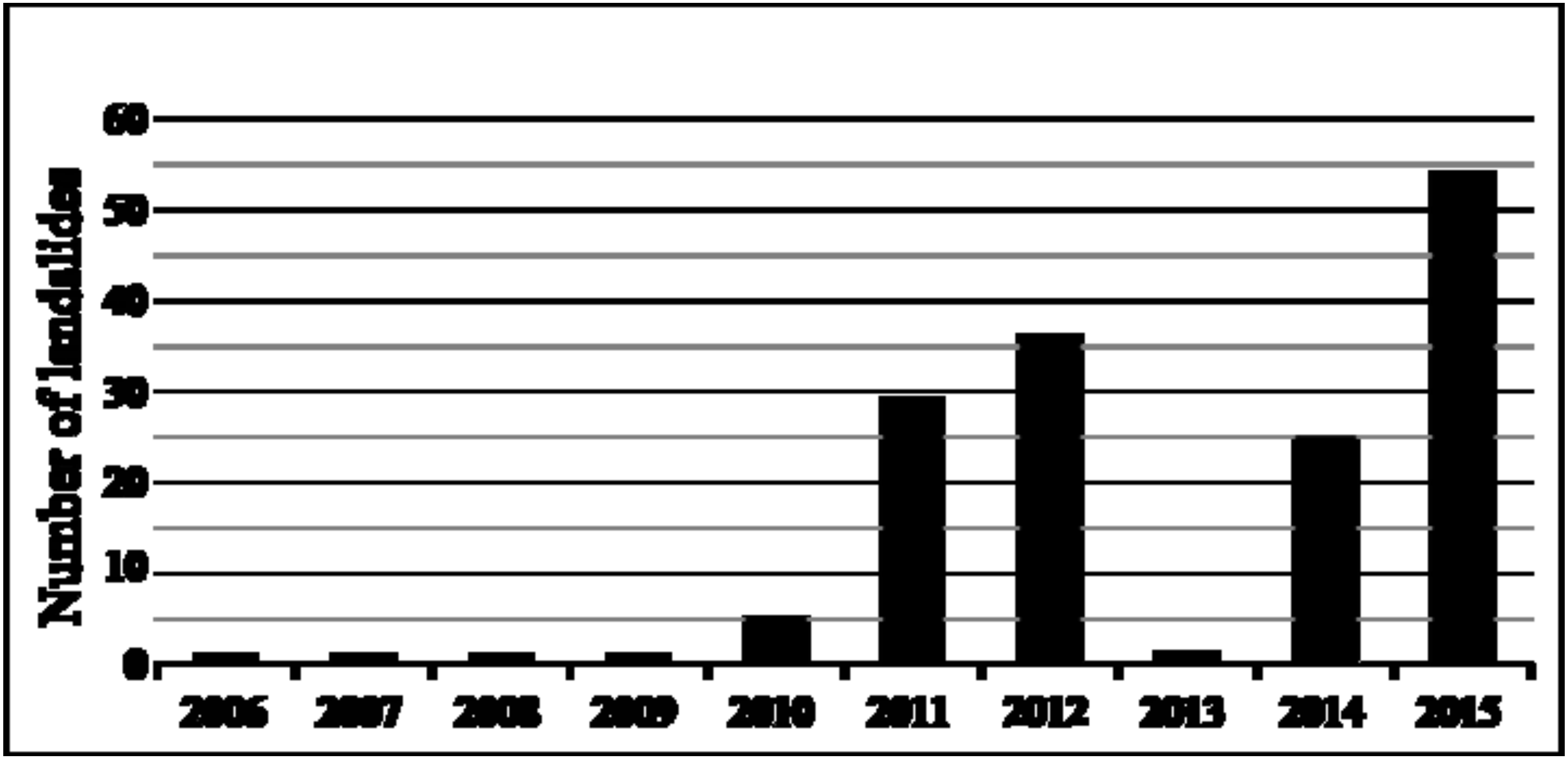

Figure 4

Trigger	Rainfall	Poor drainage	Excavation slope	Stream socavation	Unreported
Landsides	151	2	11	2	1

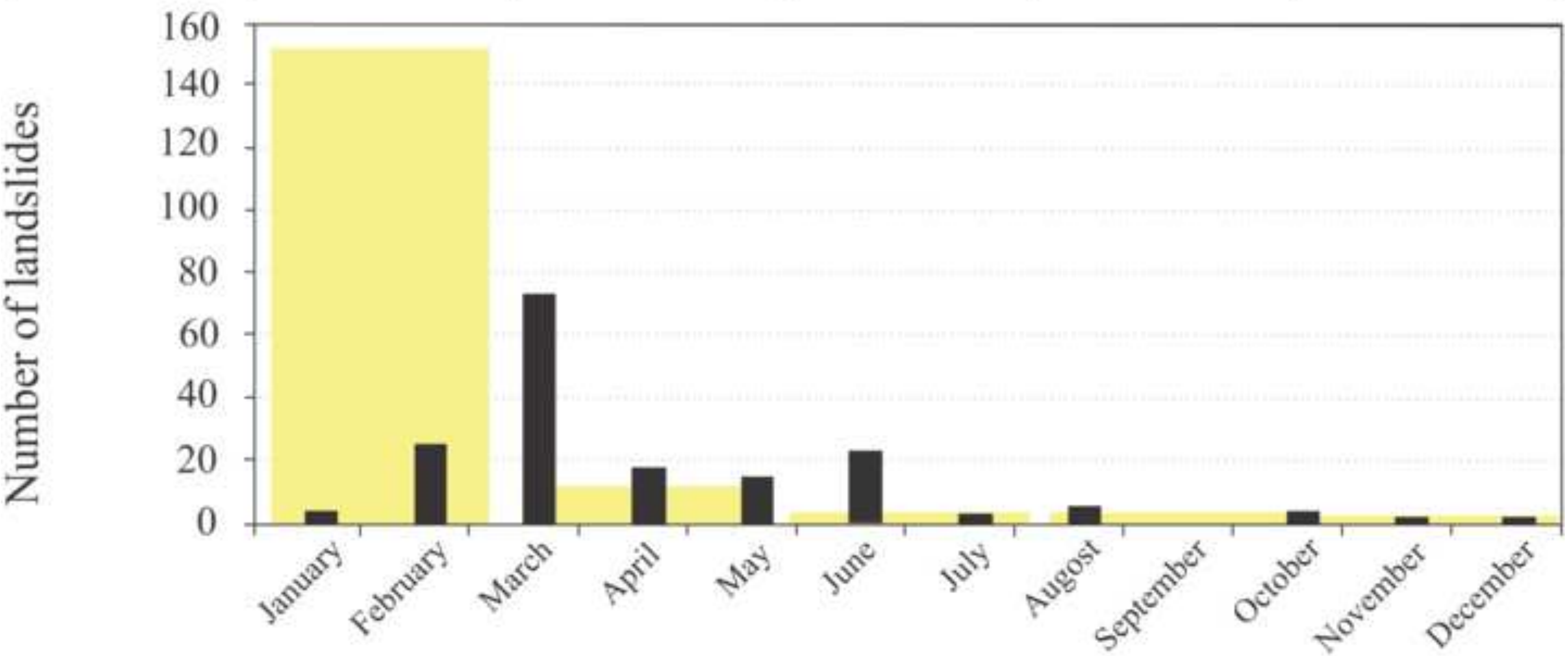

Landsides	January	February	March	April	May	June	July	Augost	September	October	November	December
	3	25	74	17	14	22	2	5	---	3	1	1

Figure 5 Click here to download Figure Figure 5.tif

Figure 6

Click here to download Figure Figure 6.tif

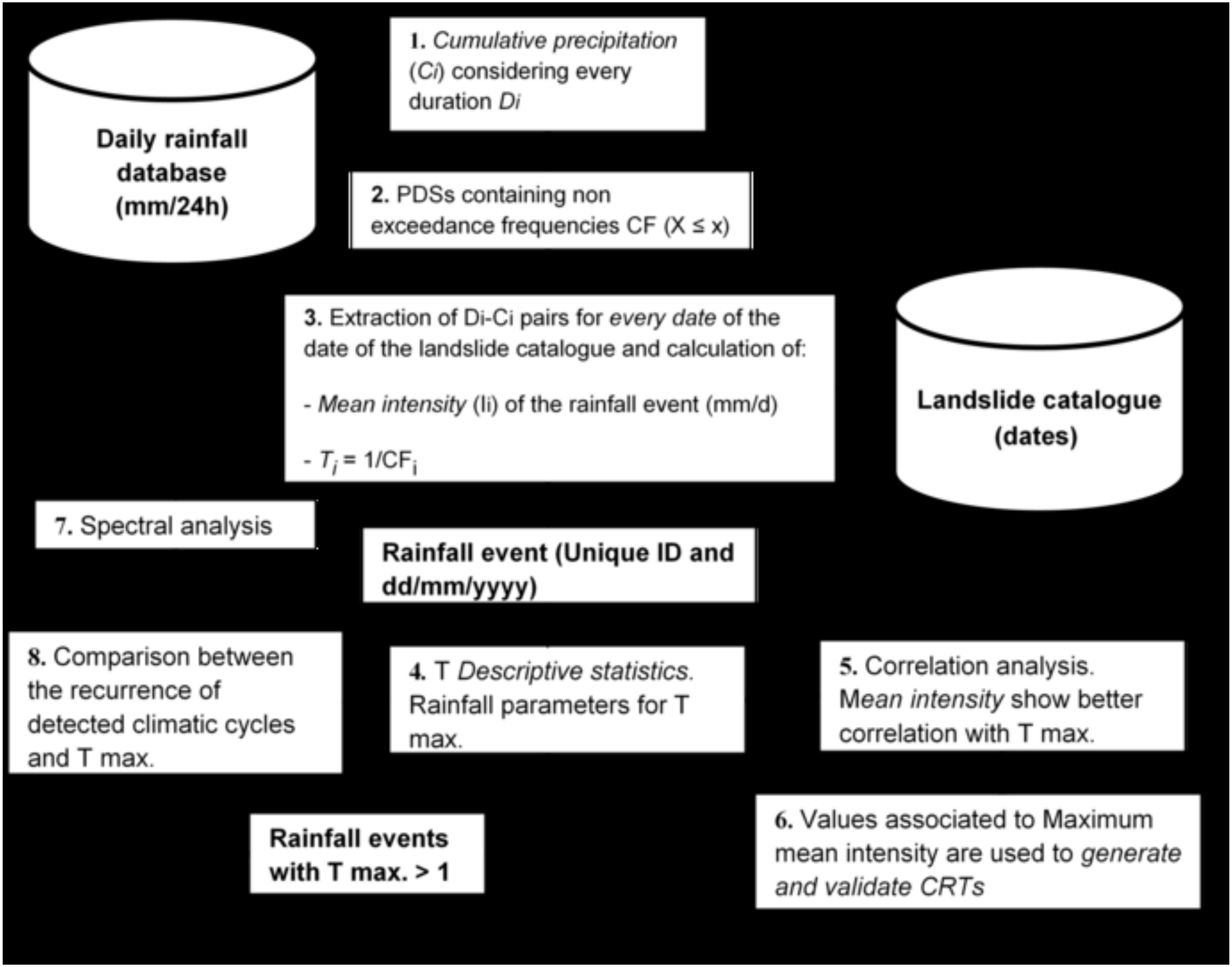

Figure 7

Click here to download Figure Figure 7.tif

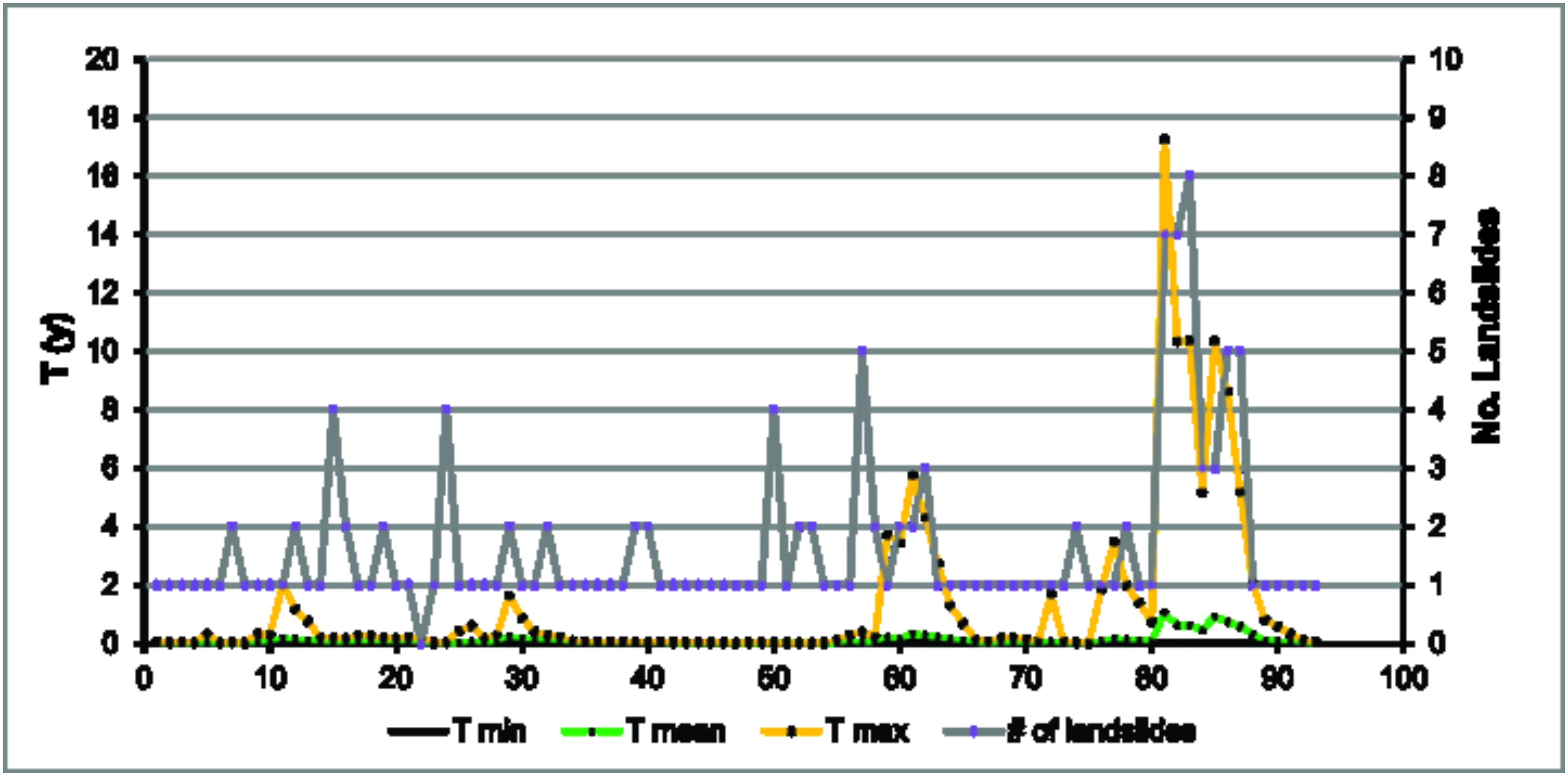

Figure 8

Click here to download Figure Figure 8.tif

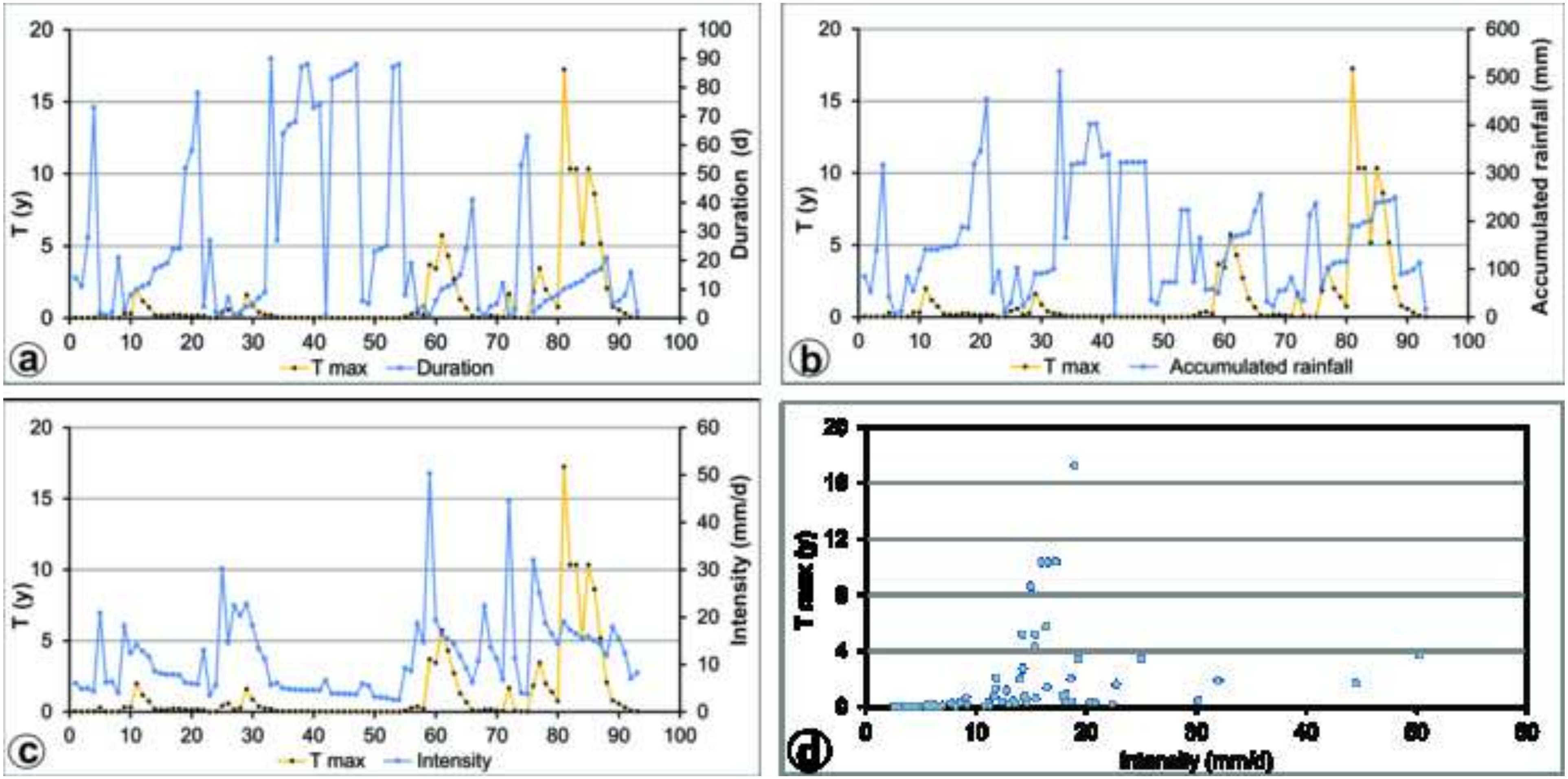

Figure 9

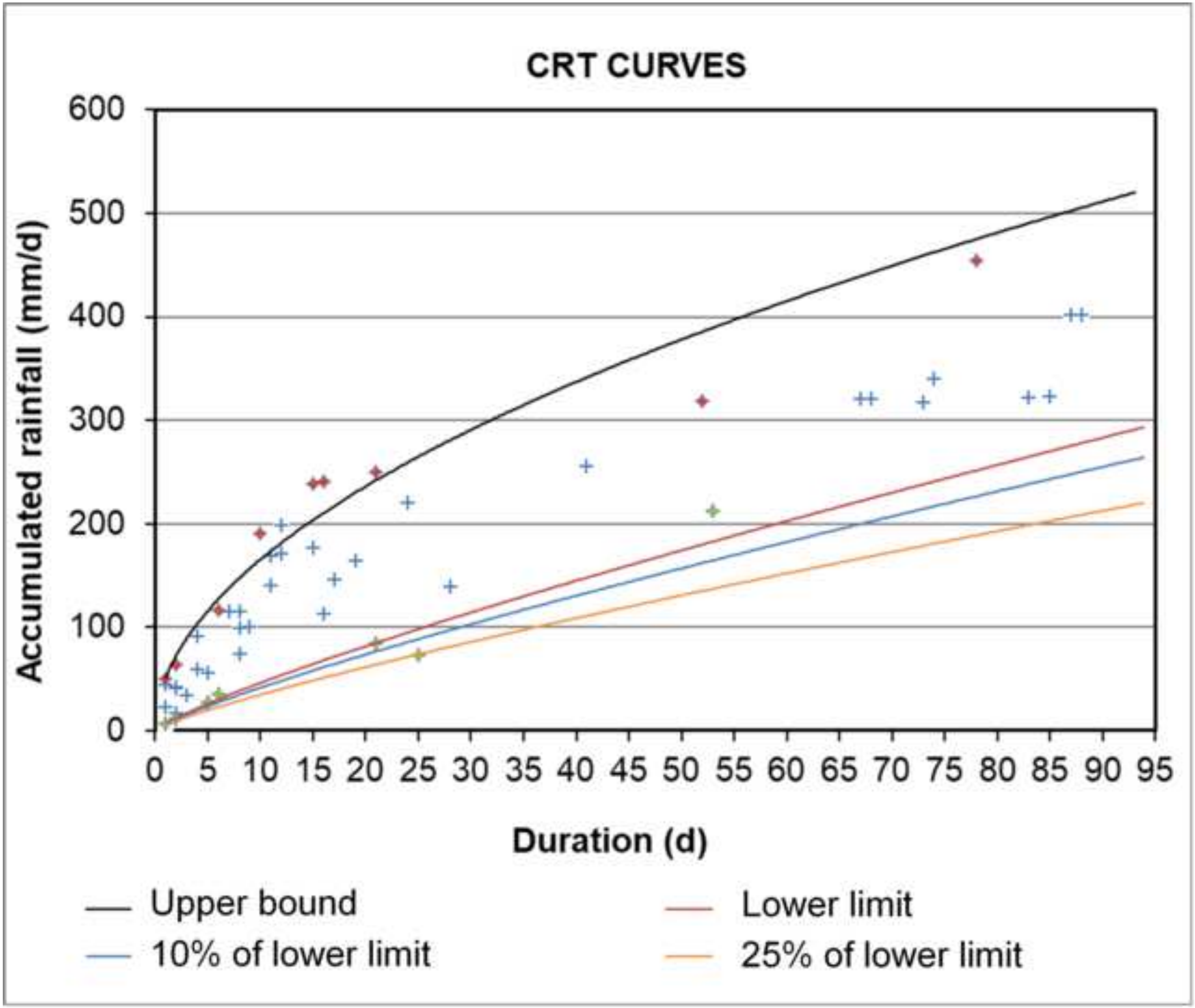
CRT CURVES
Accumulated rainfall (mm/d)
600
500
400
300
200
100
0
0 5 10 15 20 25 30 35 40 45 50 55 60 65 70 75 80 85 90 95
Duration (d)
Upper bound
Lower limit
10% of lower limit
25% of lower limit

Figure 10

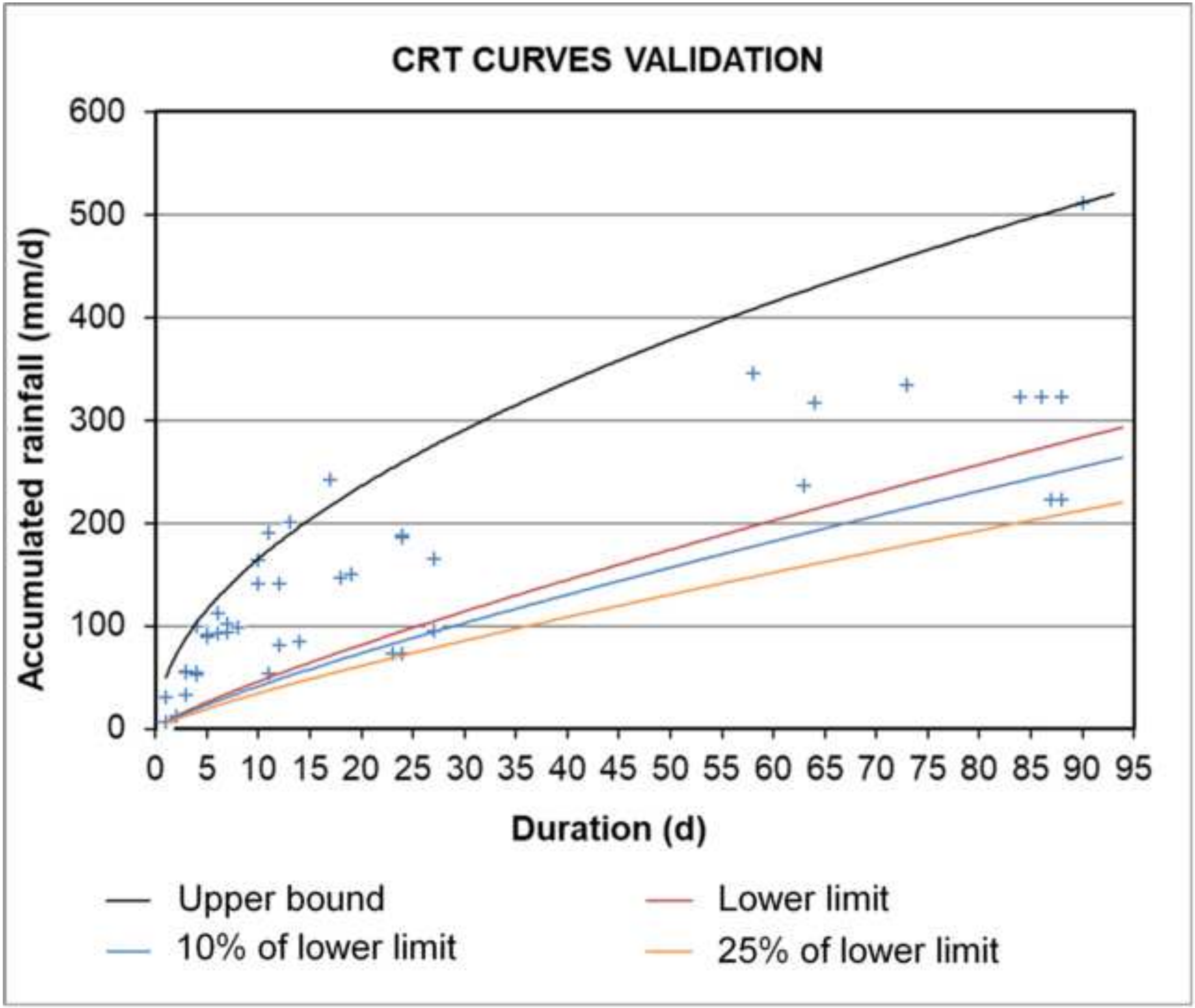

CRT CURVES VALIDATION
Accumulated rainfall (mm/d)
600
500
400
300
200
100
0
0 5 10 15 20 25 30 35 40 45 50 55 60 65 70 75 80 85 90 95
Duration (d)
Upper bound
Lower limit
10% of lower limit
25% of lower limit

Figure 11

Click here to download Figure Figure 11.tif

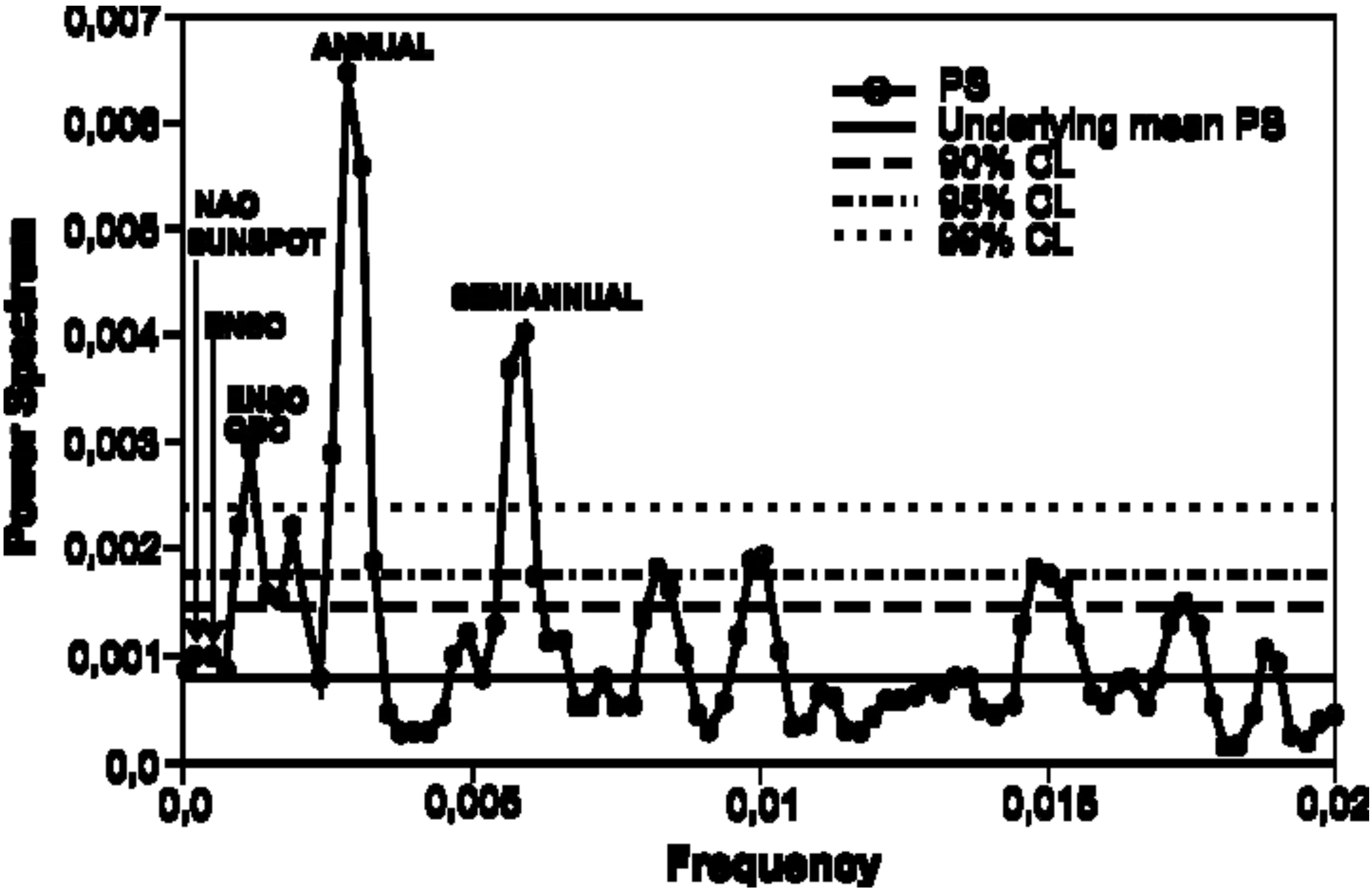

Table 1. Landslides with major damage caused in the Andean region, triggered by rainfall

Locality	Country	Year	Summary	Deaths	Damage Millon ($)	References
Vargas	Venezuela	1999	DebrisFlow	15000	4000	Salcedo en PMA 2007 Larsen & Wieczorek, 2006;
Río Limón (Aragua)	Venezuela	1987	Debrisflow	210	n/d	PMA 2007
Villatina	Colombia	1987	Earthflow	450	n/d	PMA 2007
Cerro Pucaloma (La Paz)	Bolivia	2003	Traslational	69	n/d	PMA 2007
Mayunmarca	Perú	1974	Traslational/flow	600	n/d	PMA 2007
Antofagasta	Argentina	1991	DebrisFlow	91	n/d	PMA 2007
Antofagasta Santiago Ranco Lake	Chile	1991 1993 2004	Debrisflows	130	71	Sepúlveda et al. 2006
Chunchi	Ecuador	1983	n/d	150	n/d	Petley et al. 2005
The Josefina	Ecuador	1993	Flow	35	147	Petley et al. 2005; Cadier et al. 1996; Zevallos et al. 1996

Table 2. Reported damage due to landslides in the Loja basin between 2010 and 2015 (SNGR – Zona 7)

Types of damage	Quantity	Approximate costs	Number of landslides
Affected people	1913		global
Deaths	7	unquantifiable	2
Destroyed houses	40	2000000	11
Partially affected housing	219	1095000	105
Affectation of the roads	620 meters		33
Affectation of water pipes	no reported		8
No affections reported			8
Total			**167**

Table 3. Dates for the 22 rainfall events experiencing the greatest associated return period

Date	T max. (y)	Date	T max. (y)
26/03/2015	17,3	05/03/2014	3,5
27/03/2015	10,4	11/03/2014	2,7
28/03/2015	10,4	06/04/2015	2,1
31/03/2015	10,3	22/03/2015	2,0
01/04/2015	8,6	15/02/2011	2,0
09/03/2014	5,8	18/03/2015	1,8
29/03/2015	5,2	25/10/2014	1,7
02/04/2015	5,2	28/02/2012	1,6
10/03/2014	4,3	23/03/2015	1,4
04/03/2014	3,7	14/03/2014	1,3
20/03/2015	3,5	16/02/2011	1,2

Table 4. Pearson correlation coefficient (r) between pluviometric variables (duration, accumulated rainfall and mean intensity) and T max

	T max.	Dur. (d)	Accum. rainfall (mm)	Mean int. (mm/d)
T max.	1,00			
Dur. (d)	-0,22	1,00		
Accum. rainfall (mm)	0,07	0,87	1,00	
Int. (mm/d)	0,36	-0,56	-0,41	1,00

Table 5. Correspondence between some of the rainfall events that generated landslides with known climatic cycles: solar cycle (SUNSPOT), El Niño Southern Oscillation (ENSO) and Quasi-Biennial Oscillation (QBO)

Event No.	Date	T max. (Y)	Corresponding cycle
11	15/02/2011	2,0	QBO
29	28/02/2012	1,6	QBO
61	09/03/2014	5,8	ENSO
63	11/03/2014	2,7	QBO
72	25/10/2014	1,7	QBO
76	18/03/2015	1,8	QBO
78	22/03/2015	2,0	QBO
82	27/03/2015	10,4	SUNSPOT
83	28/03/2015	10,4	SUNSPOT
84	29/03/2015	5,2	ENSO
85	31/03/2015	10,3	SUNSPOT
87	02/04/2015	5,2	ENSO
88	06/04/2015	2,1	QBO